Theory of oscillations in STM conductance caused by subsurface defects (Review Article)

Ye. S. Avotina and Yu. A. Kolesnichenko[a)]

B. Verkin Institute for Low Temperature Physics and Engineering of the National Academy of Sciences of Ukraine, 47 Lenin Ave., Kharkov 61103, Ukraine

J. M. van Ruitenbeek

Kamerlingh Onnes Laboratorium, Universiteit Leiden, Postbus 9504, 2300 Leiden, The Netherlands

(Submitted April 20, 2010)
Fiz. Nizk. Temp. **36**, 1066–1084 (October–November 2010)

In this review we discuss recent theoretical studies of single subsurface defects by means of a scanning tunneling microscope (STM). These investigations are based on quantum interference effects between the electron partial waves that are directly transmitted through the contact and the partial waves scattered by a defect. In particular, we demonstrate the feasibility of imaging the position of a defect below a metal surface by means of STM. Different types of subsurface defects are discussed: point-like magnetic and nonmagnetic defects, magnetic clusters in a nonmagnetic host metal, and nonmagnetic defects in an *s*-wave superconductor. The effect of Fermi surface anisotropy is analyzed. Studies of the effect of high magnetic fields on the STM conductance of tunnel point contacts in the presence of a single defect are also discussed.
 [doi:10.1063/1.3514417]

I. INTRODUCTION

Over the three decades following its invention,[1] scanning tunneling microscopy (STM) has proved to be a superbly valuable tool for investigating surfaces on an atomic scale. Along with mapping the surface of a conductor, STM enables the observation of many phenomena, including electron scattering by single surface defects (impurity atoms, adatoms, or step edges). Hundreds of studies of surface defects by STM have been published. We do not aim to review all of them here, but confine ourselves to brief mention of the major areas of research in this field. Our attention will be focused mainly on interference effects in STM conductance measurements caused by subsurface defects.

Electron scattering by defects leads to quantum-interference patterns in the local electron density of states around the defects (Friedel oscillations[2]). For more than thirty years Friedel oscillations were a theoretical prediction found only in theory textbooks.[3] The development of STM has made it possible to visualize of these oscillations, which manifest themselves as oscillations in the differential tunneling conductance, $G=dI/dV$, around defects on a surface.

Standing wavelike patterns in the STM conductance in the vicinity of defects were first observed by Crommie *et al.*[4] on a Cu(111) surface and by Hasegawa *et al.*[5] on a Au(111) surface. At the (111) surface of the noble metals Cu, Ag, and Au the electrons of the surface states form a quasi-two-dimensional nearly-free electron gas with an isotropic dispersion law.[6] When scattered from step edges or adatoms, the surface states form standing waves which result in an oscillatory dependence of the tunneling conductance measured as a function of the distance r_0 between the STM tip and the defect. The period of the conductance oscillations $r_0 = 2\pi/2k_F^{2D}$ is equal to twice the Fermi wave vector, $2k_F^{2D}$ ($\mathbf{k}_F^{2D}$ is a two-dimensional vector in the plane of the surface).

The circular 2D Fermi contour of the electrons at the (111) surface of noble metals results from the fact that the layer of surface atoms actually corresponds to one of the close-packed stackings on which the face-centered cubic structure is based. Generally, for less closely packed surfaces and conductors having a complicated crystallographic structure the 2D Fermi contour is anisotropic, i.e., the absolute value of the vector $\mathbf{k}_F^{2D}$ depends on its direction. The Fourier transform (FT) of the standing wave pattern provides an image of the Fermi contour. Anisotropic Friedel- like oscillations have been observed by FT-STM on Cu(110) surfaces,[7] Be,[8] and $ErSi_2$.[9] In particular, in Ref. 7 a contour related to a "neck" in the bulk Fermi surface for a Cu(110) surface was imaged.

Magnetic adatoms on nonmagnetic host metal surfaces are of special interest as they produce a characteristic many-body resonance structure in the differential conductance near zero voltage bias attributable to the Kondo effect.[10–13] The shape of the resonance in the differential conductance is usually asymmetric and is described by a Fano line shape.[14–16] The surface electron waves carry information on the magnetic impurity and, by focusing the waves, it has been possible to create a mirage image of the impurity[17] (for a review, see Ref. 18). The interesting phenomenon of an orbital Kondo resonance has been observed by STM in Ref. 19. It was found that STM images of a Cr(001) surface show cross-like depressions centered around the impurities corresponding to the orbital symmetry of two degenerate surface states d_{xz} and d_{yz}.[19]

Examining defects near the surface of unconventional superconductors by STM is a way to determine the symmetry of the order parameter. The effect of single Zn defects on the superconductivity in high-T_c superconductors has been investigated in Ref. 20, and *d*-wave pairing symmetry was observed in the quasibound state near the defect. In Ref. 21 a bound state near a magnetic Mn adatom on the surface of superconducting Nb has been observed by STM.

An effective way to enhance the sensitivity of STM to these oscillation effects is to use a superconducting tip.[22] In Ref. 23 it has been shown that the amplitude of conductance oscillations is significantly enhanced when a superconducting tip is used, and when the applied bias is close to the gap energy of the superconductor.

The applicability of STM can be extended to the study of magnetic objects on the surface of a conductor when a magnetic material is used for the STM tip so that the electric current is spin polarized (SP) (for review of SP-STM see Ref. 24). For example, the precession of the magnetic moment of clusters of organic molecules on a surface gives rise to a time modulation of the SP-STM current, from which the g-factor can be derived.[25,26] The possibility of probing the magnetic properties of nanostructures buried beneath a metallic surface by means of local probe techniques is discussed in Ref. 27. It has been shown that those properties can be deduced from the spin-resolved local density of states above the surface.[27]

STM spectroscopy also provides information on the structure of the metal below the surface in both semiconductors and metals. Crampin[28] proposed using the surface states for imaging subsurface impurities. However, exponential decay of the wave function amplitude on moving into the bulk limits the effective range to the topmost layers only, and bulk states form a good alternative for detecting defect positions. The principle of imaging subsurface defects is based on the influence on the conductance caused by quantum interference of electron waves that are scattered by defects and reflected back by the contact. This effect was explored for investigating subsurface Ar bubbles submerged in Al[29] and Cu,[30] and Si(111) step edges buried under a thin film of Pb.[31] In these experiments, bulk electrons were found to be confined in a vertical quantum well between the surface and the top plane of the object of interest. The observation of interference patterns due to electron scattering by Co impurities in the interior of a Cu sample has been reported Refs. 32 and 33.

Reviews of the theory of STM can be found in Refs. 34 and 35. The papers cited there in which the conductance of a tunnel contact of small size was analyzed theoretically, should be supplemented by the fundamental paper by Kulik, Mitsai, and Omelyanchouk[36] published in 1974. On the basis of rigorous quantum-mechanical considerations, the authors of that paper obtained an analytical formula for the conductance of a junction between two metal half-spaces separated by an inhomogeneous tunnel barrier of low transparency. Their result is valid for arbitrary values of the applied bias and for an arbitrary dependence of the tunneling probability on the coordinates in the plane of the interface between the metals. As a special case, the general formula for the contact resistance can be applied to inhomogeneous tunnel contacts with characteristic diameters smaller than the electron wave length; this is appropriate for describing the STM conductance. Recently, electron tunneling through a randomly inhomogeneous barrier of arbitrary amplitude has been analyzed theoretically in Refs. 37 and 38.

In most papers, the theoretical description of STM conductance oscillations owing to electron scattering by single defects is based on the assumption that the tunneling conductance measured by the STM tip is proportional to the local density of states (LDOS) $\upsilon(\mathbf{r})$ of the sample,[18,28,39,40] as in the case of a planar tunnel junction.[41] For surface scattering of electrons this assumption is quite reasonable, but for electron scattering in the bulk of a sample it cannot be used. The LDOS in the vicinity of defects in the bulk is critically modified by electron reflections off the surface of the conductor, i.e., at $\mathbf{r}\in\Sigma$, and differs from Friedel oscillations of the LDOS in an infinite conductor with a single scatterer.[3] In the limit of zero tunneling probability we have $\upsilon(\boldsymbol{r}\in\Sigma)=0$. In addition, the conductance oscillations are formed only by "tagged" electrons, which tunnel through the contact and are scattered back by the defect, while a "halo" of Friedel oscillations around the defect is caused by all the scattered electrons. In general, there are no other periods in the interference effects except that of the Friedel oscillations, $\Delta r_0 = 2\pi/2k_F$ ($\mathbf{k}_F$ is the Fermi wave vector), and the analysis in Ref. 33 of the experimental data in terms of a bulk LDOS seems to be qualitatively correct.[42] However, calculating the amplitudes and phases of the conductance oscillations, which contain additional information on the interaction of the charge carriers with the defect, requires solving the scattering problem including the effect of subsurface defects on the conductance of a small tunnel contact.

In this paper we review a series of publications on the theory of electron transport though a tunnel point contact when a single defect exists below the metal surface. This paper is organized as follows: a model of tunnel contacts and the basic equations describing the effect of subsurface defects on STM conductance measurements are given in section II. The solution of the Schrödinger equation for elections that tunnel through the contact and are scattered by the defect is given. In section III a method is formulated for determining the positions of defects below a metal surface based on a study of the nonlinear conductance of a contact. The signature of a Fermi surface anisotropy in STM conductance in the presence of subsurface defects is discussed in section IV. In section V we summarize the results of investigations of the effect of a subsurface magnetic defect on the tunnel current, including the signature of a Kondo impurity and that of a magnetic cluster with an unscreened magnetic moment. In section VI it is shown that a strong magnetic field leads to specific magneto-quantum oscillation periods which depend on the distance between the contact and the defect. The feasibility of studying the interference of quasiparticles in a superconductor is analyzed in section VII. In section VIII we conclude by discussing the prospects for exploiting these theoretical results for subsurface imaging and in experimental studies of the physical characteristics of subsurface defects.

II. QUANTUM INTERFERENCE OF SCATTERED ELECTRON WAVES IN THE VICINITY OF A POINT CONTACT

A. Model of STM contacts and the Schrödinger equation for these systems

As a model for the STM experiments we choose an inhomogeneous tunnel contact between two metal half spaces

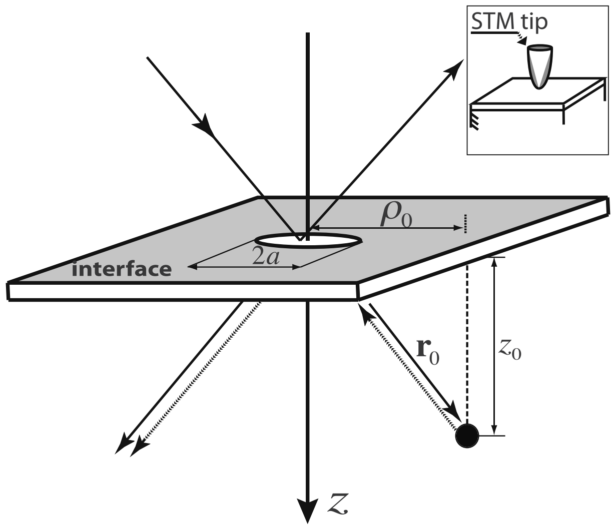

FIG. 1. Model of a tunnel point contact as an orifice in an interface that is nontransparent for electrons except for a circular hole, where tunneling is allowed. Trajectories are shown schematically for electrons that are reflected from or transmitted through the contact and then scattered back by a defect.

separated by an infinitely thin interface. The potential barrier in the plane of the interface, at $z=0$, is chosen to have a delta function form,[36]

$$U(\mathbf{r}) = U_0 f(\rho)\delta(z), \tag{1}$$

where $\boldsymbol{\rho}$ is the radius vector in the plane of the interface, perpendicular to the z axis. The function $f(\rho)\to\infty$ at all points of the plane $z=0$ except for a small region defining the contact, which has a characteristic radius a, at which $f(\rho)$ is of order 1. As an example, a suitable model for the function $f(\rho)$ for the "STM tip" is the Gaussian function $f(\rho) = \exp(\rho^2/a^2)$ with small a. Another useful model for a junction is an orifice of radius a for which $f(\rho)=1$ for $\rho \leqslant a$ in the plane of the contact (Fig. 1).

Of course, a model of this sort only describes the qualitative features of the conductance at an STM contact, and does not include such parameters as the tip radius, or the distance between the STM tip and the sample, as, for example, in the model of Tersoff and Hamann.[43] In principle these properties of the system may be included in the model as parameters of the function $f(\rho)$. The advantage of the model by Kulik, *et al.*[36] is the possibility of finding exact analytical solutions of the Schrödinger equation in the limit $U_0\to\infty$. The equations are considerably simplified for a small contact with $a\to 0$. The wave functions obtained using the model barrier (1) properly describe the spreading of electron waves into the bulk metal from a small region on its surface. A numerical value for the STM conductance plays the role of a scale factor for the conductance oscillations, but it is of lesser importance following discussion.

A defect in the vicinity of the interface can be described by the potential

$$D(\mathbf{r}) = gD_0(|\mathbf{r}-\mathbf{r}_0|), \tag{2}$$

where g is a constant for the electron interaction with the defect, and $D_0(|\mathbf{r}-\mathbf{r}_0|)$ is a spherically symmetric function localized within a region of characteristic radius r_D centered at the point $\mathbf{r}=\mathbf{r}_0$, which satisfies the normalization condition

$$4\pi\int dr' r'^2 D_0(r') = 1. \tag{3}$$

The electron wave function $\psi(\mathbf{r})$ in a metal with the dispersion relation $\varepsilon(\mathbf{k})$ must be found from the Schrödinger equation[44]

$$\left[\varepsilon\left(\hat{\mathbf{k}} - \frac{e}{c\hbar}\mathbf{A}\right) + \sigma g_e \mu_{\mathrm{B}} H + eV(\mathbf{r}) + D(\mathbf{r}) + U(\mathbf{r})\right]\psi = \varepsilon\psi. \tag{4}$$

Here $\hat{\mathbf{k}} = -i\nabla$ is the vector-potential of the stationary magnetic field $\mathbf{H}$, and $V(\mathbf{r})$ is the applied electrical potential, $\sigma = \pm 1$ corresponds to different spin directions, $\mu_B = e\hbar/2m_0c$ is the Bohr magneton, where m_0 is the free electron mass, and g_e is the electron g-factor. The function $\psi(\mathbf{r})$ satisfies the following boundary condition for continuity of the wave function at $z=0$:

$$\psi(\rho,+0) = \psi(\rho,-0), \tag{5}$$

as well as the condition, which for a δ-function barrier is obtained by the integration of the Schrödinger equation (4) over an infinitesimal interval near the point $z=0$,

$$\int_{-0}^{+0} dz\varepsilon\left(\hat{\mathbf{k}} - \frac{e}{ch}\mathbf{A}\right)\psi(\rho,z) = -U_0 f(\rho)\psi(\rho,0). \tag{6}$$

In the next section we consider a solution of Schrödinger equation (4) for a free electron model with an effective electron mass m^* and a dispersion relation $\varepsilon(\mathbf{k}) = 2\mathbf{k}^2/2m^*$ in the absence of external fields ($H=0$, $V=0$). In this case, the condition (6) reduces to the well-known condition on the discontinuity in the derivative of the wave function

$$\psi_z'(\rho,+0) - \psi_z'(\rho,-0) = \frac{2m^* U_0}{h^2} f(\rho)\psi(\rho,0). \tag{7}$$

The effects of applied voltage, Fermi surface anisotropy, and magnetic field are discussed in the following sections.

B. Wave function for an inhomogeneous tunnel barrier

Here we follow the procedure for the finding the electron wave function in the limit $U_0\to\infty$ proposed in Ref. 36. To a first approximation in the small parameter $1/U_0$ the wave function $\psi(\mathbf{r})$ can be written as

$$\psi(\mathbf{r}) = \psi_0(\mathbf{r}) + \varphi_0(\mathbf{r}), \tag{8}$$

where ϕ_0 is of order $1/U_0$. This latter part of the wave function (8) describes electron tunneling through the barrier and determines the electrical current. The first term in Eq. (8) is the solution of the Schrödinger equation for the metallic half-spaces without the contact,

$$\psi_0(\mathbf{r}) = \mathrm{e}^{i\kappa\mathbf{r}}(\mathrm{e}^{ik_z|z|} - \mathrm{e}^{-ik_z|z|}), \tag{9}$$

where $\boldsymbol{\kappa}$ and k_z are the components of the wave vector $\mathbf{k}$ parallel and perpendicular to the interface, respectively. Equation (9) satisfies the boundary condition $\psi_0(\rho,0)=0$ at the interface.

On substituting the wave function (8) into the boundary conditions (5) and (6), we must match terms of the same order in $1/U_0$. As a result, the conditions (5) and (6) reduced to[36]

$$\varphi_0(\rho,+0)=\varphi_0(\rho,-0), \tag{10}$$

and

$$t(k_z)\mathrm{e}^{i\kappa\mathbf{r}}=f(\rho)\varphi_0(\rho,0), \tag{11}$$

where

$$t(k_z)=\hbar^2 k_z/im^* U_0; \quad |t|\ll 1, \tag{12}$$

is the amplitude of the electron wave function passing through the homogeneous barrier. Expanding the function $\varphi_0(\rho,z)$ as a Fourier integral in the coordinate ρ, and using Eq. (11), we obtain[36]

$$\varphi_0(\rho,z\gtrless 0)=\frac{t(k_z)}{(2\pi)^2}\int_{-\infty}^{\infty}d\kappa'\mathrm{e}^{i\kappa'\rho+ik_z'|z|}\int_{-\infty}^{\infty}d\rho'\frac{\mathrm{e}^{i(\kappa-\kappa')\rho'}}{f(\rho')}, \tag{13}$$

where $k_z'=\sqrt{k^2-\kappa'^2}$. For a homogeneous δ-function barrier $(\rho)=1$, Eq. (13) transforms into a transmitted plane wave with amplitude t.

The characteristic radius of the region on the surface through which electrons tunnel from the STM tip into the sample is of atomic size, $a\simeq 0.1$ Å, while the Fermi wave vector $k_F\simeq 1$ Å^{-1}. On using the condition $k_F a\ll 1$, after integrating over $\boldsymbol{\kappa}'$ and ρ' in Eq. (13), we find[46]

$$\varphi_0(\mathbf{r})=t(k_z)\frac{i(ka)^2 z}{2r}h_1^{(1)}(kr). \tag{14}$$

An incident plane wave is transformed into a spherical p-wave $h_1^{(1)}(kr)$ (Eq. (14)) after scattering by the point contact. In Eq. (14), and below, the $h_1^{(1)}(x)$ are the spherical Hankel functions. Note that the wave function $\varphi_0(\mathbf{r})$ (14) is zero at all points on the surface $z=0$, except at the point $r=0$ (at the contact), where it diverges. This divergence is the result of taking the limit $a\to 0$ in the integral expressions for $\varphi_0(\mathbf{r})$ (13). Nevertheless, Eq. (14) gives a finite value for the total charge current through the contact upon integration over a half-sphere of radius r with its center in the point $r=0$ in the limit $r\to 0$.

C. Electron scattering by a single defect in the vicinity of a tunnel point contact

Because of current spreading, only a small region near the point contact has a significant effect on the conductance. For high purity samples only a few defects will be found in this region. At low temperatures the distance between the contact and the nearest defect, $r0$, is smaller than the electron mean free path due to electron–phonon scattering and the electrons are elastically scattered by the single defect only. The wave function of transmitted electrons, $\phi(\mathbf{r})$, which takes into account the scattering by the defect, can be expressed in terms of the retarded Green function $G_0^+(\mathbf{r},\mathbf{r}';\varepsilon)$ of the homogeneous equation (4) at $D=0$, in the absence of impurity scattering. To first approximation in the transmission amplitude t (12) the integral equation for $\phi(\mathbf{r})$ is given by

$$\varphi(\mathbf{r})=\varphi_0(\mathbf{r})+g\int d\mathbf{r}'D(|\mathbf{r}'-\mathbf{r}_0|)G_0^+(\mathbf{r},\mathbf{r}',\varepsilon)\varphi(\mathbf{r}'), \tag{15}$$

where

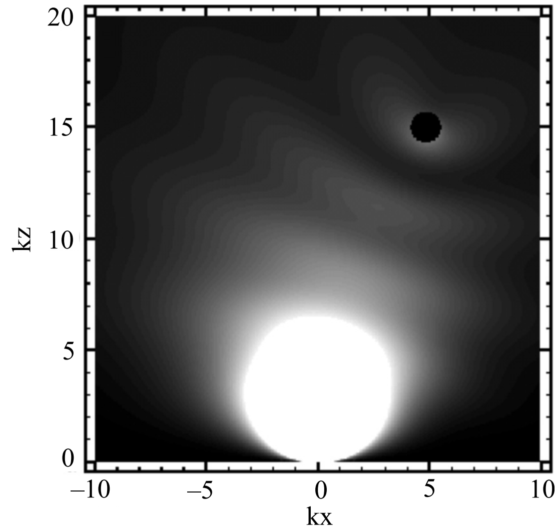

FIG. 2. Spatial distribution of the square of the modulus of the wave function in the vicinity of a contact in a plane perpendicular to the interface passing through the contact and a defect. Distances are given in units of the inverse wave number.[47]

$$G_0^+(\mathbf{r},\mathbf{r}';\varepsilon)=-\frac{ikm^*}{2\pi\hbar^2}\{h_0^{(1)}(k|\mathbf{r}-\mathbf{r}'|)-h_0^{(1)}(k|\mathbf{r}-\tilde{\mathbf{r}}'|)\}, \tag{16}$$

is the electron Green function of Eq. (4) for the semi-infinite half-space $(U_0\to\infty)$, $\bar{\mathbf{r}}'-(\rho',-z')$, and $\rho_0(\mathbf{r})$ is given by Eq. (13). For small g, Eq. (15) can be solved using perturbation theory, i.e., in first approximation in g the function $\varphi(\mathbf{r}')$ in the integral term should be replaced by $\varphi_0(\mathbf{r}')$.

For a short range potential $(kr_D\ll 1)$ the function $\varphi(\mathbf{r}')$ can be taken outside of the integral in Eq. (15) and the scattered wave function can be written in the form[45]

$$\varphi(\mathbf{r})=\varphi_0(\mathbf{r})+T(k)\varphi_0(\mathbf{r}_0)G_0^+(\mathbf{r},\mathbf{r}_0;\varepsilon), \tag{17}$$

where

$$T(k)=\frac{g}{1-g\displaystyle\int d\mathbf{r}'D_0(|\mathbf{r}'-\mathbf{r}_0|)G_0^+(\mathbf{r}_0,\mathbf{r}';\varepsilon)}. \tag{18}$$

Note that Eq. (17) is valid far from the defect $(|\mathbf{r}-\mathbf{r}_0|\gg r_0)$ and the function $D_0(|\mathbf{r}'-\mathbf{r}_0|)$ must converge for the integral in the denominator of Eq. (18) as $\mathbf{r}'\to\mathbf{r}_0$. It is well known that s-wave scattering is dominant for scattering by a short range potential and the scattering matrix (18) can be expressed in terms of the s-wave phase shift δ_0[46] as

$$T(k)=\frac{i\pi\hbar^2}{m^*k}\frac{\mathrm{e}^{2i\delta_0}-1}{1+(1/2)(\mathrm{e}^{2i\delta_0}-1)h_0^{(1)}(2kz_0)}. \tag{19}$$

The effective T-matrix is an oscillatory function of the distance z_0 between the defect and the interface that results from repeated electron scattering by the defect after reflections from the interface. Figure 2 illustrates the spatial distribution of the square of the modulus of the wave function (17) in the vicinity of a contact with a defect located at $\mathbf{r}_0=(5,0,15)/k$.

III. FRIEDEL-LIKE OSCILLATIONS OF THE TUNNEL POINT-CONTACT CONDUCTANCE

A. Voltage dependence of the STM conductance

In the case of low transparency (12), the applied voltage drops over the entire barrier and the electrical potential can be chosen to be a step function $V(\mathbf{r})=V\Theta(-z)$. At zero temperature, electrons tunnel to the lower half-space when $eV>0$, while for $eV<0$ electrons can tunnel only to available states in the upper half-space (Fig. 1).

The tunneling current $I(V)=I^{(-)}(V)-I^{(-)}(V)$ is the difference between two currents flowing through the contact in opposite directions. Each of these currents can be evaluated by means of the probability current density $J_k^{(\pm)}(V)$ integrated over the plane z=const, and then integrating over all directions of the electron wave vector

$$J_k^{(\pm)}(V)=\nu(\varepsilon)\int_{-\infty}^{\infty}d\rho\Theta(\pm z)\mathrm{Re}\langle\Theta(\pm k_z)\varphi^*(\mathbf{r})\hat{v}_z\varphi(\mathbf{r})\rangle_\varepsilon, \tag{20}$$

where $\nu(\varepsilon)$ is the electron density of states for one spin direction, $(\ldots)_\varepsilon$ denotes the average over an iso-energy surface $\varepsilon(\mathbf{k})=\varepsilon$:

$$\langle\ldots\rangle_\varepsilon=\left(\int_{\varepsilon(\mathbf{k})=\varepsilon}\frac{dS_k}{|\mathbf{v}|}\right)^{-1}\int_{\varepsilon(\mathbf{k})=\varepsilon}\frac{dS_\mathbf{k}}{|\mathbf{v}|}\ldots, \tag{21}$$

$dS_\mathbf{k}$ is an element of the iso-energy surface in $\mathbf{k}$-space, and $\hat{\mathbf{v}}=(1/h)\partial\varepsilon(\hat{\mathbf{k}})/(\partial\hat{\mathbf{k}})$ is the velocity operator. In a free-electron model for the energy spectrum, $\hat{v}_z=(h/im^*)(\partial/\partial z)$. The voltage dependence of the current density $J_k^{(\pm)}(V)$ (20) is determined by the dependence of the absolute value of the wave vector for an electron incident on the contact, $|\mathbf{k}(V)|=\sqrt{k^2-2m^*|eV|/h^2}$.

The total current through the contact is

$$I(V)=e\sum_{\alpha=\pm1}\int d\varepsilon[J_k^{(+)}(V)f_F(\varepsilon-eV)(1-f_F(\varepsilon))-J_k^{(-)}\times(V)f_F(\varepsilon)(1-f_F(\varepsilon-eV))], \tag{22}$$

where $f_F(\varepsilon)$ is the Fermi function.

The current-voltage characteristic $I(V)$ is calculated by substituting the wave function (17) into Eq. (20) and taking Eqs. (13), (16), and (19) into account. Retaining only terms of first order in g (i.e., ignoring multiple scattering at the impurity site; in Eq. (17) $T(k)\sim g$), and in the limit of low temperatures, $T=0$, the conductance $G(V)=dI/dV$ can be written as[47]

$$G(\mathbf{r}_0,V)=\frac{e^2\hbar^3}{4\pi^3(m^*U_0)^2}\int\int\frac{d\rho_1d\rho_2}{f(\rho_1)f(\rho_2)}\times\left[k_F^2\tilde{k}_F^4F_{\tilde{k}_F}(\rho_1,\rho_2)-2\int_{k_F}^{\tilde{k}_F}k^5dkF_k(\rho_1,\rho_2)\right], \tag{23}$$

where

$$F_k(\rho_1,\rho_2)=\left[\frac{j_1(k\rho)}{k\rho}\right]^2-\frac{4m^*gk}{\pi\hbar^2}\frac{j_1(k\rho)}{k\rho}\frac{z_0^2}{\lambda_1\lambda_2}j_1(k\lambda_1)y_1(k\lambda_2), \tag{24}$$

$\rho=|\rho_1-\rho_2|$, $\lambda_1=\sqrt{z_0^2+|\rho_0-\rho_1|^2}$, $\lambda_2=\sqrt{z_0^2+|\rho_0-\rho_2|^2}$, $y_l(x)$ and $y_l(x)$ are the spherical Bessel functions, and

$$\tilde{k}_F(V)=\sqrt{k_F^2+2m^*eV/\hbar^2} \tag{25}$$

is the Fermi wave vector k_F accelerated by the potential difference. For concreteness, a positive sign of the bias is chosen in Eq. (23), i.e., $eV>0$.

If the contact radius $a\ll\lambda_F$ ($\lambda_F=1/k_F$ is the Fermi wave length), then Eq. (23) for the conductance can be simplified to

$$G(\mathbf{r}_0,V)=G_0\left\{q\left(\frac{eV}{\varepsilon_F}\right)-\tilde{g}\frac{z_0^2}{r_0^2}\left[\left(\frac{\tilde{k}_F}{k_F}\right)^5w(\tilde{k}_Fr_0)-\left(\frac{\tilde{k}_F}{k_F}\right)^7v(\tilde{k}_Fr_0)+v(k_Fr_0)\right]\right\}, \tag{26}$$

where

$$G_0=|t(k_F)|^2\frac{e^2(k_Fa)^4}{36\pi h} \tag{27}$$

is the inherent conductance of the tunnel point contact, $r_0=\sqrt{z_0^2+|\rho_0|^2}$,

$$q(x)=1+x-\frac{1}{3}x^3, \tag{28}$$

$$w(x)=\frac{1}{x^4}[(x^2-1)\sin 2x+2x\cos 2x], \tag{29}$$

$$v(x)=\frac{1}{x^7}[2x(4x^2-7)\sin 2x+(2x^4-14x^2+7)\cos 2x], \tag{30}$$

and

$$\tilde{g}=\frac{6m^*k_F}{\pi\hbar^2}g \tag{31}$$

is the dimensionless interaction constant.

Equation (26) describes the oscillations of the STM conductance as a function of the distance r_0 between the STM tip and the subsurface defect, and as a function of the bias eV. For distances between the contact and the defect $r_0\gg\lambda_F$ and $eV\ll\varepsilon_F$, the oscillatory dependence becomes sinusoidal

$$G(\mathbf{r}_0,V)-G_0\propto\frac{z_0^2}{r_0^4}\sin 2\tilde{k}_Fr_0. \tag{32}$$

Voltage dependent oscillations of the STM conductance owing to quantum interference caused by impurity scattering, have been observed by Untiedt *et al.*,[48] and Ludoph *et al.*[49]

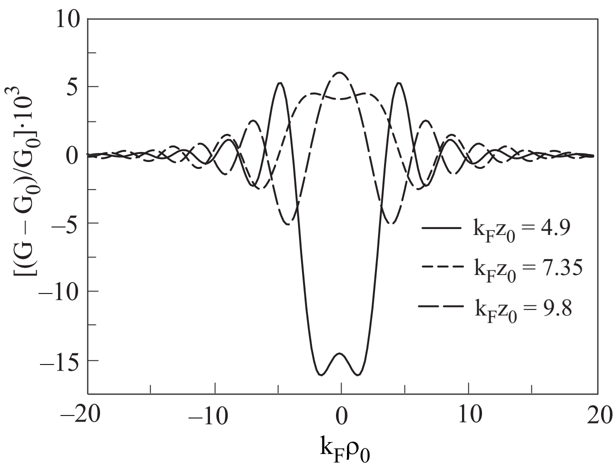

FIG. 3. Dependence of the normalized oscillatory part of the conductance on the STM tip position for different depths z_0 of the defect below the surface; $\mathbf{r}_0=(\rho_0,0,z_0)$, $g=1$.

B. Determination of the defect positions

We now discuss whether this effect can be exploited experimentally for three dimensional mapping of subsurface impurities. The position of the defect in a plane parallel to the surface can be found by analyzing the oscillatory pattern in the dependence $G(\rho_0)$. In most cases the center of this pattern corresponds to a tip position directly above the defect, $\rho_0=0$. A possible effect owing to the Fermi surface anisotropy is discussed in the next section. Note that, in contrast to the case of surface defects, the oscillations (26) in the conductance are not periodic in the tip distance ρ_0 along the surface, but their period is defined by the distance $r_0=\sqrt{\rho_0^2+z_0^2}$. Generally, the depth z_0 can be found by fitting the experimental data to the theoretical dependence $G(\rho_0,z_0)$ (26). Figure 3 illustrates the oscillatory component of $G(\rho_0,V=0)$ as a function of ρ_0 for different choices of z_0. In this plot we have taken $g=1$, the Fermi wave vector $k_F=1.360$ Å^{-1}, and the interatomic distance $d=1.805$ Å for Cu. Thus, the plots correspond to defect positions in the third, fourth, and fifth layers below the Cu surface. The $G(\rho)$ curves closely resemble the observations by Quaas *et al.*[32] for Co atoms embedded in Cu(111).

For determining the defect depth z_0 one can use the periodicity in the phase $\vartheta=2\tilde{k}_F r_0$ of $G(r_0,V)$ (32) for sufficiently large r_0. According to Eq. (32), at $V=0$ two sequential radii ρ_{01} and ρ_{02}, with $\rho_{02}>\rho_{01}$, corresponding to neighboring maxima (or minima), satisfy the obvious condition of periodicity, $\Delta\vartheta=2k_F(\sqrt{\rho_{02}^2+z_0^2}-\sqrt{\rho_{01}^2+z_0^2})=2\pi$. For known k_F this is a simple algebraic equation for z_0, which yields

$$z_0=\frac{1}{2\pi k_F}\sqrt{k_F^4(\rho_{02}^2-\rho_{01}^2)^2-2\pi^2k_F^2(\rho_{02}^2+\rho_{01}^2)+\pi^4}. \quad (33)$$

Note that $k_F(\rho_{02}-\rho_{01})>\pi$ and the radicand is positive. A second way of changing the product $\tilde{k}_F r_0$ is by varying the maximum value of the electron wave vector through the applied voltage.

A first approach for determining the defect depth z_0 from the bias dependence of the period of the Friedel-like oscillations of the STM conductance has been described by Kobayashi.[42] The depth z_0 can estimated by tracking the point ρ_0 while changing the bias voltage $|eV|$, keeping the phase of the oscillations, ϑ, constant: $k_F\sqrt{\rho_0^2+z_0^2}=\tilde{k}_F(V)\sqrt{\rho_0'^2+z_0^2}$, where ρ_0 and ρ_0' are the positions corresponding to two different bias voltages $V\to 0$ and $V_2=V$ with the same phase (for example, a fixed maximum).[42] The solution of the above equation with $\tilde{k}_F(V)$ (25) gives

$$z_0=\sqrt{\frac{\varepsilon_F(\rho_0^2-\rho_0'^2)-eV\rho_0'^2}{eV}}, \quad (34)$$

where $eV>0$ and $\rho_0>\rho_0'$.

The method proposed in Ref. 47 has certain advantages. If the STM tip is placed above the defect ($|\rho_0|\ll z_0$) the conductance amplitude decreases with the depth of the defect as z_0^2, which offers the hope of observing defects at substantial distances below the surface. The depth of an impurity can be obtained from the $G(V)$ curve at $\rho_0=0$, which shows oscillations in eV with a period $e\Delta V$, and gives

$$z_0=\frac{x}{k_F-\tilde{k}_F(\Delta V)}. \quad (35)$$

In a real experiment it is not necessary to observe a full period of $G(V)$; for example, a quarter period will be sufficient for determining the defect depth.[47]

IV. SIGNATURE OF THE FERMI SURFACE ANISOTROPY

In most metals the dispersion relation for the charge carriers is a complicated anisotropic function of momentum. This leads to anisotropy of the various kinetic characteristics.[44] In particular, as shown in Ref. 50, the current distribution may be highly anisotropic in the vicinity of a point contact. This effect influences the way the point contact conductance depends on the position of the defect. For example, in the case of a Au(111) surface the "necks" in the Fermi surface (FS) should cause a defect to be invisible when probed exactly from above.

The wave function of electrons injected by a point contact for arbitrary FS $\varepsilon(\mathbf{k})=\varepsilon_F$ has been analyzed qualitatively by Kosevich.[50] He noted that at large distances from the contact the electron wave function for a certain direction $\mathbf{r}$ is defined by those points on the FS for which the electron group velocity is parallel to $\mathbf{r}$. Unless the entire FS is convex there are several such points. The amplitude of the wave function depends on the Gaussian curvature K in these points, which can be convex ($K>0$) or concave ($K<0$). The parts of the FS with curvatures having different signs are separated by $K=0$ contours (inflection lines). In general there is a continuous set of electron wave vectors for which $K=0$. The electron flux in directions with zero Gaussian curvature exceeds the flux in other directions.[50]

Electron scattering by defects in metals with an arbitrary FS can be highly anisotropic.[44] Generally, the wave function of the electrons scattered by a defect consists of several superimposed waves, which travel with different velocities. In the case of an open FS there are directions along which the electrons cannot move at all. Scattering events along those directions occur only if the electron is transferred to a different sheet of the FS.[44]

In this section we analyze the effect of anisotropy of the FS on the signals used to determine the position of a defect below a metal surface by STM. We shall show that the amplitude and period of the conductance oscillations are determined by the local geometry of the FS, namely by those points for which the electron group velocity is directed along the radius vector from the contact to the defect. The general results are illustrated for the FS of noble metals.

Initially, we do not specify the specific form of $\varepsilon(\mathbf{k})$, except that it satisfies the general condition of point symmetry $\varepsilon(\mathbf{k})=\varepsilon(-\mathbf{k})$. In the reduced zone scheme a given vector $\mathbf{k}$ identifies a single point within the first Brillouin zone. As for an isotropic FS, the electron wave function $\psi(\mathbf{r})$ in the metal with an arbitrary dispersion relation can be found at $U_0\to\infty$ by using the method described in section III. The boundary conditions for the transmitted wave function $\varphi_0(\mathbf{r})$ have the same form as Eqs. (10) and (11) with the function $t(\mathbf{k})$ replaced by

$$t(\mathbf{k})=\frac{1}{U_0}\left[\int dz\varepsilon\left(\boldsymbol{\kappa},\frac{\partial}{i\partial z}\right)(\mathrm{e}^{ik_z|z|}-\mathrm{e}^{-ik_z^{\mathrm{ref}}|z|})\right]_{z=-0}. \tag{36}$$

In the free electron model, Eq. (36) transforms into Eq. (12). For electrons incident on the contact, the components of $\mathbf{k}$ perpendicular to the interface, $k_z(\boldsymbol{\kappa},\varepsilon)$, and reflected from the contact, $k_2^{\mathrm{ref}}(\boldsymbol{\kappa},\varepsilon)$, are related by the conditions expressing the conservation of energy ε and the tangential component $\boldsymbol{\kappa}$ of the wave vector, i.e.,

$$\varepsilon(\boldsymbol{\kappa}^{\mathrm{in}},k_z)=\varepsilon(\boldsymbol{\kappa}^{\mathrm{ref}},k_z^{\mathrm{ref}})=\varepsilon;\quad \boldsymbol{\kappa}^{\mathrm{in}}=\boldsymbol{\kappa}^{\mathrm{ref}}\equiv\boldsymbol{\kappa}. \tag{37}$$

The wave function scattered by the defect is defined by the general relation (15).

General expressions for the STM conductance into a metal with an arbitrary FS can be found in Ref. 51. Here, we give simplified asymptotic expressions for the oscillatory part of the conductance $\Delta G_{\mathrm{osc}}^{\mathrm{arb}}(\mathbf{r}_0)$ (the difference between the total conductance and its value without a defect) which are valid for large distances between the contact and the defect, $r_0\gg\lambda_F$,

$$\Delta G_{\mathrm{osc}}^{\mathrm{arb}}(\mathbf{r}_0)=\frac{2ge^2a^4z_0^2}{hr_0^4}\nu(\varepsilon_F)\langle|t(\mathbf{k})|^2\Theta(v_z)\rangle_{\varepsilon_F}$$
$$\times\sum_{s,s'}\frac{1}{\sqrt{|K(\mathbf{k}_{0s})K(\mathbf{k}_{0s'})|}}\sin(h(\mathbf{k}_{0s})r_0$$
$$+\phi_s)\cos(h(\mathbf{k}_{0s'})r_0+\phi_{s'}). \tag{38}$$

All functions of the wave vector in Eq. (38) are taken at the points of the FS for which the electron group velocity $\mathbf{v}_0$ is parallel to the vector $\mathbf{r}_0=r_0\mathbf{n}_0$, $h(\varepsilon_F,\mathbf{k}_0)=\mathbf{k}_0\mathbf{n}_0$, $\mathbf{k}_0$ is the wave vector corresponding to the point on the FS at which $\mathbf{v}_0\|\mathbf{n}_0$. The function $h(\varepsilon_F,\mathbf{k}_0)$ is well known in differential geometry as the support function of the surface $\varepsilon(\mathbf{k})=\varepsilon_F$.[52] If the curvature of the FS changes sign, there is more than one point $\mathbf{k}_{0s}$ $(s=1,2\ldots)$ for which $\mathbf{v}_{0s}\|\mathbf{n}_0$. It may also occur that for certain directions of the vector $\mathbf{r}_0$, $\mathbf{v}\|\mathbf{n}_0$ for all points on the FS, and the electrons cannot propagate along these directions.[44] For these $\mathbf{r}_0$, the oscillatory part of the conductance is zero.

In Eq. (38)

$$\phi=\frac{\pi}{4}\,\mathrm{sgn}\left(\frac{\partial^2k_z^{(+)}}{\partial k_x^2}\right)(1+\mathrm{sgn}\,K(\mathbf{k}_0)), \tag{39}$$

$\langle\ldots\rangle_{\varepsilon_F}$ is defined by Eq. (21), $k_z^{(+)}=k_z^{(+)}(k_x,k_y,\varepsilon_F)$ at the point defined by the direction of the vector $\mathbf{n}_0$ in $\mathbf{k}$-space, $K(\mathbf{k}_0)\neq0$ is the Gaussian curvature of the FS given by

$$K(\varepsilon_F,\mathbf{k}_0)=\frac{\hbar^2}{|\mathbf{v}_0|^2}\sum_{i,j=x,y,z}A_{ik}n_{0i}n_{0j}, \tag{40}$$

$A_{ij}=\partial\det(\mathbf{m}^{-1})/\partial m_{ij}^{-1}(\mathbf{k})$ is the algebraic adjunct of the element $m_{ij}^{-1}(\mathbf{k})=(1/\hbar^2)(\partial^2\varepsilon/\partial k_i\partial k_j)$ of the inverse mass matrix $\mathbf{m}^{-1}$.

Equation (38) is valid if the curvature $K\neq0$. The amplitude of the electron wave function in a direction of zero Gaussian curvature is larger than in other directions. This results in an enhanced current flow near the conical surface defined by the condition $K=0$.[50,51] If the FS is open, there are directions along which electron flow does not occur. These properties of the wave function manifest themselves in the oscillatory part of the conductance (38): (i) The amplitude of the oscillations is maximal if the direction from the contact to the defect corresponds to the electron velocity associated with an inflection line. (ii) There are no conductance oscillations, i.e., $\Delta G_{\mathrm{osc}}^{\mathrm{arb}}=0$, if this direction corresponds to cones within which electron motion is forbidden.

For an ellipsoidal FS the Schrödinger equation can, in fact, be solved exactly in the limit of $a\to0$ and $U_0\to\infty$, and the conductance of the contact can be found for arbitrary distances between the contact and the defect. For this FS the dependence of the electron energy ε on the wave vector $\mathbf{k}$ is given by

$$\varepsilon(\mathbf{k})=\frac{\hbar^2}{2}\sum_{i,j=x,y,z}\frac{k_jk_i}{m_{ij}}, \tag{41}$$

where the k_i are the components of the electron wave vector $\mathbf{k}$, and the $1/m_{ij}$ are constants representing the components of the inverse effective mass tensor $\mathbf{m}^{-1}$.

To within the first order in g (i.e., ignoring multiple scattering at the impurity site), the conductance in the limit $V\to0$[51] is given by

$$G^{\mathrm{ell}}(\mathbf{r}_0)=G_0^{\mathrm{ell}}\left[1-\frac{6g(2\varepsilon_F)^{3/2}}{\pi\hbar^5\sqrt{m_{zz}}\det[\mathbf{m}^{-1}]}\right.$$
$$\left.\times\left(\frac{z_0}{h(\mathbf{k}_0)r_0}\right)^2w(h(\mathbf{k}_0)r_0)\right], \tag{42}$$

where G_0^{eff} is the conductance in the absence of a defect ($g=0$):[51]

$$G_0^{\mathrm{ell}}=\frac{2e^2a^4\varepsilon_F^3}{9\pi\hbar^3U_0^2\sqrt{m_{zz}}\det[\mathbf{m}^{-1}]}, \tag{43}$$

$$h(\mathbf{k}_0)=\frac{1}{\hbar}\left(\frac{2\varepsilon_F}{\det[\mathbf{m}^{-1}]}\sum_{i,j=x,y,z}A_{ij}n_{0i}n_{0j}\right)^{1/2}, \tag{44}$$

and $w(kr)$ is given by Eq. (29).

The center of the oscillatory pattern of the conductance, $G^{\mathrm{ell}}(\mathbf{r}_0)$, as a function of the tip position ρ_0 corresponds to $\rho_0=\rho_{00}$ with respect to the contact point at $\mathbf{r}=0$, where

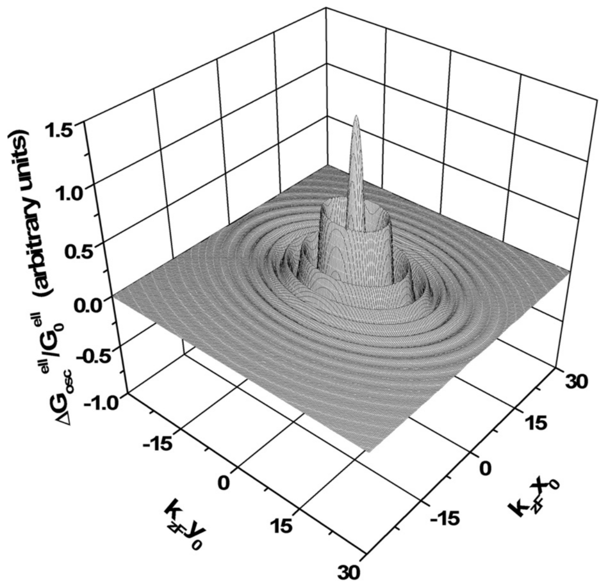

FIG. 4. Dependence of the oscillatory part of the conductance, $AG_{\rm osc}^{\rm cell}$, as a function of the position of a defect ρ_0 in the plane $z=z_0$. The shape of the FS (41) is defined by the mass ratios $m_x/m_z=1$, $m_y/m_z=3$, and the long axis of the ellipsoid is rotated by $\pi/4$ about the x axis, away from the y axis. The coordinates are measured in units of $1/k_{zF}$ (46) and the defect lies at $z_0=5$.[51]

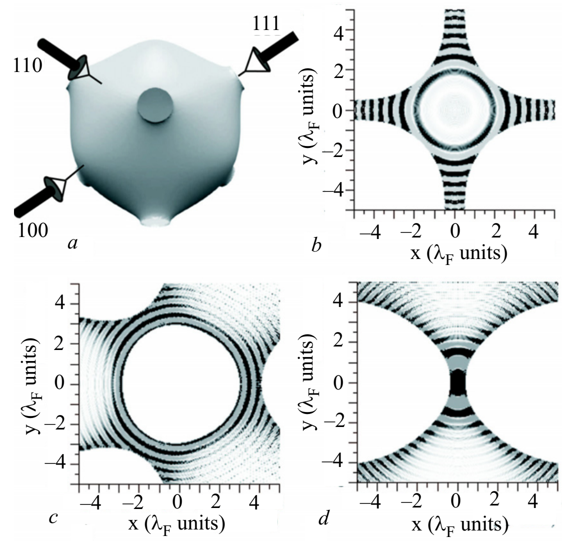

FIG. 5. (a) The Fermi surface given by Eq. (48) relative to the contact axis for three principal lattice orientations. (b) A plot of the tunneling point-contact conductance G as a function of the contact position for a defect at the origin, at a depth of $5\lambda_F$ and for a (100) surface plane; the x and y directions each correspond to 100 directions. (c) Same plot for a (111) surface orientation; the x and y directions correspond to $[11\bar{2}]$ and $[1\bar{1}0]$ directions, respectively. (d) Same plot for a (110) surface orientation; the x and y directions correspond to $[001]$ and $[1\bar{1}0]$ directions, respectively.[69]

$$\rho_{00} = z_0\left(\frac{m_{zz}}{m_{zx}}, \frac{m_{zz}}{m_{zy}}\right). \tag{45}$$

The support function h for this tip position,

$$\mathbf{k}_0\mathbf{n}_{00} \equiv k_{zF} = \frac{1}{h}\sqrt{2\varepsilon_F m_{zz}} \tag{46}$$

corresponds to an extreme position of the chord $2k_{zF}$ of the FS in the direction normal to the interface, $\mathbf{n}_{00}$ is the unit vector in the direction of the vector $\mathbf{r}_{00}=(\rho_{00}, z_0)$. Figure 4 shows that $\Delta G_{\rm osc}^{\rm ell}=G^{\rm ell}-G_0^{\rm ell}$ is an oscillatory function of the defect position ρ_0 that reflects the ellipsoidal shape of the FS; the oscillations are largest when the contact is placed in the position ρ_{00} defined by Eq. (45).

In deriving Eq. (38), we have assumed that $eV \to 0$. For a finite voltage, but with $eV \ll \varepsilon_F$, all functions of the energy ε in Eq. (38) can be taken at $\varepsilon=\varepsilon_F$, except $h(\varepsilon, \mathbf{k}_0)$ in the oscillatory functions. When $eV \ll \varepsilon_F$,

$$h(\varepsilon_F + eV, \mathbf{k}_0) \approx h(\varepsilon_F, \mathbf{k}_0) + \frac{\partial h}{\partial \varepsilon_F} eV, \quad \frac{\partial h}{\partial \varepsilon_F} \sim \frac{k_z}{\varepsilon_F} \tag{47}$$

and when the product $(eV/\varepsilon_F)k_F r_0 \gg 1$, the conductance (38) is clearly an oscillatory function of the voltage V. The periods of the oscillations are defined by the energy dependence of $h(\varepsilon, \mathbf{k}_0)$. The results obtained properly describe the total conductance for $eV \ll \varepsilon_F$ and can also be used for analyzing the periods of the oscillations when $eV \leqslant \varepsilon_F$.

Further calculations require information about the actual shape of the FS, $\varepsilon(\mathbf{k})=\varepsilon_F$. In Ref. 51 a model FS in the form of a corrugated cylinder was considered. This model, for which analytical dependences of the conductance on the defect position can be found, described the common features of FS geometries and the conductance oscillations: anisotropy of the convex parts ("bellies"), the changes in sign of the curvature (inflection lines), and open directions ("necks").

The conductance oscillation pattern was been analyzed numerically[53] for the noble metals copper, silver and gold on the basis of Eq. (38). The parameterization of the FS was taken from Ref. 54,

$$\varepsilon(\mathbf{k}) = \alpha\left[-3 + \cos\frac{k_x a}{2}\cos\frac{k_y a}{2} + \cos\frac{k_y a}{2}\cos\frac{k_z a}{2} + \cos\frac{k_z a}{2}\cos\frac{k_x a}{2} + r(-3 + \cos k_x a + \cos k_y a + \cos k_z a)\right], \tag{48}$$

which is 99% accurate. The values for the constants are $r=0.0995$, $\varepsilon/\alpha=3.63$, and for copper, silver, and gold $a=0.361$, 0.408 nm, and 0.407 nm, respectively. The Fermi energy of copper is 7.00 eV, of silver, 5.49 eV and of gold, 5.53 eV.

The results of computations for three crystallographic orientations are shown in Fig. 5. All distances in Fig. 5 are given in units of λ_F, which is 0.46 nm for copper, and 0.52 nm for silver and gold. For each of these surface orientations the graphs have symmetries corresponding to the particular orientation of the FS. "Dead" regions, where the conductance of the contact is equal to its value without the defect and there are no conductance oscillations, can be seen in all the figures. These regions originate from the "necks" of the FS and their edges are defined by the inflection lines. For all orientations of the metal surface a defect located in the plane of the surface corresponds to a center of symmetry. The appearance of "dead" regions depends on the depth of the defect, which can be estimated in the following way: the orientations of the "neck" axes define the axes of cones with an aperture angle 2γ, within which there are no scattered electrons. The vertices of the cones coincide with the defect site. The radius R of the central "dead" region, given by $R = z_0 \tan \gamma$, is proportional to the depth of the defect.[32]

The feasibility of visualizing the Fermi surface of Cu in real space by examination of the interference patterns caused by subsurface Co atoms has been demonstrated by Weismann, *et al.*[33]

V. SUBSURFACE MAGNETIC DEFECTS

A. Kondo impurity

In the case of magnetic defects at low temperatures ($T \ll T_K$, where T_K is the Kondo temperature), the Kondo resonance produces a dramatic enhancement of the effective electron-impurity interaction[55] and perturbation methods are no longer applicable. Kondo correlations give rise to a sharp resonance in the density of states at an energy $\varepsilon(\mathbf{k}) = \varepsilon_K$ near the Fermi level. As $\varepsilon(\mathbf{k}) \to \varepsilon_K$ the effective electron scattering cross section acquires a maximum value corresponding to the Kondo phase shift $\delta_{0K} = \pi/2$.[55] In that case, multiple scattering needs to be taken into account, even for a single defect, because of electron reflection by the metal surface.

In this subsection the conductance is expressed in terms of the s-wave scattering phase shift δ_0. The results describe the effect of multiple electron scattering on the conductance, which shows up as harmonics in the variation of G with the applied voltage and with the distance between the contact and the defect. This analysis of the nonmonotonic voltage dependence of the conductance is applied specifically to the interesting problem of Kondo scattering by using an appropriate phase shift:[56]

$$\delta_0(k) = \left[\frac{\pi}{2} - \tan^{-1}\left(\frac{\varepsilon(\mathbf{k}) - \varepsilon_K}{T_K}\right)\right] + \delta_{0D}. \tag{49}$$

The first term in Eq. (49) describes resonant scattering on a Kondo impurity level ε_K (T_K is the Kondo temperature). For a nonmagnetic impurity this term is absent. The second term δ_{0D} takes the usual potential scattering into account.

Taking Eq. (17) for the wave function of a spherical Fermi surface and Eq. (19) for the scattering matrix makes it possible to find the differential conductance $G = dI/dV$ of the tunnel point contact in the approximation of s-wave scattering. For $|eV| < \varepsilon_F$ and for $eV > 0$, $G(V)$ is given by[46]

$$G(V) = G_0\left[q(V) + \left(\frac{\tilde{k}_F}{k_F}\right)^4 \Phi(\tilde{k}_F) - \frac{2}{k_F^6}\int_{k_F}^{\tilde{k}_F} dk k^5 \Phi(k)\right], \tag{50}$$

and for $eV < 0$, by

$$G(V) = G_0\left[q(V) + \left(\frac{\tilde{k}_F}{k_F}\right)^2 \Phi(\tilde{k}_F) - \frac{4}{k_F^6}\int_{k_F}^{\tilde{k}_F} dk k^3 \left(k^2 - \frac{2m^* eV}{\hbar^2}\right)\Phi(k)\right]. \tag{51}$$

Here G_0 is given by Eq. (27), $\bar{k}_F = \sqrt{k_F^2 + 2m^* eV/\hbar^2}$, and

$$\Phi(k) = F^{-1} \sin \delta_0 \frac{z_0^2}{r_0^2}[12 j_1(kr_0)(-y_1(kr_0)\cos \delta_0 + \{j_1(kr_0) \times (j_0(2kz_0) - 1) + y_0(2kz_0) y_1(kr_0)\}\sin \delta_0) + 6(1 - j_0(2kz_0))(kr_0)^{-4}(1 + (kr_0)^2)\sin \delta_0], \tag{52}$$

$$F = 1 + 2 \sin \delta_0\left[\left(\frac{1}{2(2kz_0)^2} - j_0(2kz_0)\right)\sin \delta_0 - y_0(2kz_0)\cos \delta_0\right], \tag{53}$$

$\delta_0(k)$ is the s-wave phase shift (49), and $f_l(x)$ and $y_l(x)$ are the spherical Bessel functions.

At low voltages the conductance can be represented by an expansion in the small parameter $1/(k_F z_0) < 1$,

$$G(0) = G_0\left\{1 + 12\frac{z_0^2}{r_0^2}\frac{1}{(k_F r_0)^2}\sum_{n=1}^{\infty}(-1)^n \frac{\sin^n \delta_0}{(2k_F z_0)^{n-1}} \times \left[\frac{1}{2}\left(1 - \frac{1}{(k_F r_0)^2}\right)\sin(2k_F(r_0 + (n-1)z_0) + n\delta_0) + \frac{1}{k_F r_0}\cos(2k_F(r_0 + (n-1)z_0) + n\delta_0)\right]\right\}. \tag{54}$$

The second term in Eq. (54) is a sum over n events of scattering by the defect and $n-1$ reflections by the surface. Retaining only the n=1, Eq. (54) reduces to the result obtained by perturbation theory in section III above, which is valid for $\delta_0 \simeq -gm^* k_F/2\pi\hbar^2 \ll 1$. The arguments of the sine and cosine functions in Eq. (54) correspond to the phase accumulated by the electron as it moves along semiclassical trajectories.

The voltage dependence of the conductance is not symmetric about $V=0$. This asymmetry arises from the dependences of the phase shift $\delta_0(\tilde{k}_F)$ (49) and the magnitude of the wave vector $\tilde{k}_F = \sqrt{k_F^2 + 2m^* eV/\hbar^2}$ on the sign of eV. The physical origin of this asymmetry comes from the fact that the scattering amplitude depends on the electron energy in the lower half-space (see Fig. 1), where the defect is situated. This energy is different for different directions of the current.

It is noteworthy that the sign of the Kondo anomaly depends on the distance r_0 between the contact and the defect. This distance, together with the value of the wave vector $\tilde{k}_F$, determines the period of the oscillations in $G(V)$. If the bias eV_K coincides with a maximum in the oscillatory part of the conductance, then the sign of the Kondo anomaly is positive and *vice versa*, i.e., the sign of the Kondo anomaly is negative at a minimum in the periodic variation of $G(V)$.

Figure 6 illustrates the difference $\delta G_K(V)/G_0 = (G_m - G_n)/G_0$ between the voltage dependences for magnetic G_m and nonmagnetic G_n impurities with the same potential scattering intensity. Figure 6 illustrates the evolution of the shape of the Kondo anomaly for several values of the distance between the contact and an impurity lying on the contact axis. Varying the distance changes the periodicity of the normal-scattering oscillations, which causes a change of sign in the Kondo signal. A similar dependence of the differential conductance on the distance between an STM tip and an adatom

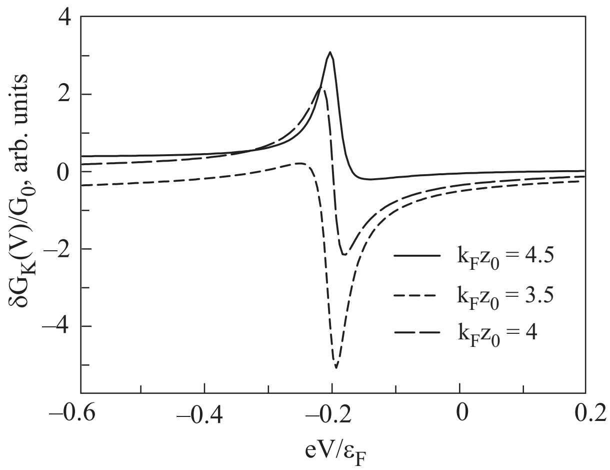

FIG. 6. The difference $\delta G_K(V)/G_0$ between the conductance as a function of voltage for a magnetic and a nonmagnetic impurity. The parameters $\varepsilon_K = 0.9\varepsilon_F$, $T_K = 0.01\varepsilon_F$, and $\delta_{0D} = 0.1$ are used in Eq. (49) and (46).

on the surface of a metal has been obtained theoretically in Refs. 57 and 58 using an Anderson impurity Hamiltonian.[59] We have obtained a Fano-like shape of the Kondo resonance in the framework of a single-electron approximation,[46] while many-body effects have been taken into account in Refs. 57 and 58.

B. Magnetic cluster

In this subsection we consider the influence of a defect having an unscreened magnetic moment on the conductance of a tunnel point contact between magnetic and nonmagnetic metals in a spin-polarized scanning tunneling microscope (SP-STM) geometry.[24] A magnetic cluster is assumed to be embedded in a nonmagnetic metal in the vicinity of the contact. As first predicted by Frenkel and Dorfman[60] particles of a ferromagnetic material are expected to organize into a single magnetic domain below a critical particle size (a typical value for this critical size for Co is about 35 nm). Depending on the size and the material, the magnetic moments of such particles can be $\mu_{\mathrm{eff}} \sim 10^2 - 10^5\ \mu_B$.[61]

In general, the moment $\boldsymbol{\mu}_{\mathrm{eff}}$ of a cluster in a nonmagnetic metal can have an arbitrary direction. This direction can be held fixed by an external magnetic field $\mathbf{H}$, given roughly by $H \simeq T/\mu_{\mathrm{eff}}$, where T is the temperature (see, for example, Ref. 61). For $\mu_{\mathrm{eff}} \simeq 10^2\ \mu_B$ and $T \sim 1$ K the field H is of order 0.01 T. If H is much higher than the magnetocrystalline anisotropy field of the magnetic STM tip, then the direction of the external magnetic field controls the direction of the cluster magnetic moment, but its influence on the spin polarization of the tunnel current is negligible. In this case the magnetic moment μ_{eff} of the cluster is "frozen" by the field H and the problem becomes time independent.

If the external magnetic field is sufficiently weak and the radius of the electron trajectories $r_H = \hbar c k_F / eH$ is much greater than the distance r_0 between the contact and the cluster, the effects owing to modulation of the tunnel current caused by electron spin precession[62] and trajectory magnetic effects[63] are negligible.

The geometry of a SP-STM experiment can be described in terms of the model presented in Fig. 1, where the half-space $z<0$ is taken up by a ferromagnetic conductor with magnetization $\mathbf{M}$. In Ref. 64 the direction of the vector $\mathbf{M}$, which defines the direction of the polarization of tunnel current is chosen to be along the z axis. In real SP-STM the polarity of the STM current is defined by the magnetization of the last atom of the tip.[24] A magnetization oriented along the contact axis can be obtained, for example, with a Fe/Gd-coated W STM tip.[65]

The interaction potential $\hat{D}(\mathbf{r})$ of the electrons with the cluster is a matrix consisting of two parts,

$$\hat{D}(\mathbf{r}) = \left(g\hat{I} + \frac{1}{2\mu_B} J \mu_{\mathrm{eff}} \hat{\sigma} \right) D_0(|\mathbf{r} - \mathbf{r}_0|), \tag{55}$$

where g is a constant describing the nonmagnetic part of the interaction (for $g>0$ the potential is repulsive), J is the constant for the exchange interaction, $\boldsymbol{\mu}_{\mathrm{eff}} = \mu_{\mathrm{eff}}(\sin\alpha, 0, \cos\alpha)$ is the magnetic moment of the cluster, $\hat{\boldsymbol{\sigma}} = (\hat{\sigma}_x, \hat{\sigma}_y, \hat{\sigma}_z)$ and $\hat{\sigma}_\mu$ are the Pauli matrices, and $\hat{I}$ is the unit matrix. The function $D_0(r)$ satisfies the condition (3). In the case of spin-flip scattering, the spinor electron wave functions satisfy the Schrödinger equation (4), where the scattering potential must be replaced by the matrix $\hat{D}(\mathbf{r})$ (55). Assuming that the potential $\hat{D}(\mathbf{r})$ and the transparency of the tunnel barrier in the contact plane are small, the two-component wave function can be found by the method described in section II.

The difference in the magnitudes of the wave vectors $\mathbf{k}_\sigma$ for spin-up and spin-down electrons (for the same energy ε), which move towards the contact from the ferromagnetic side,

$$k_{\uparrow\downarrow} = \frac{1}{\hbar} \sqrt{2m^*(\varepsilon \mp 4\pi g_e \mu_B M)}, \tag{56}$$

results in different amplitudes $t_\sigma = t(\mathbf{k}_\sigma)$ (see Eq. (12)) for electron waves injected into a nonmagnetic metal with different directions of the spin (g_e is the electron g-factor). The total effective polarization P_{eff} of the current depends on the difference between the tunneling probabilities for the different σ, i.e.,

$$P_{\mathrm{eff}}(\varepsilon) = \frac{|t_\uparrow|^2 - |t_\downarrow|^2}{|t_\uparrow|^2 + |t_\downarrow|^2}. \tag{57}$$

The conductance G of the contact at $T=0$ and $eV \ll \varepsilon_F$ is given by[64]

$$G = \frac{I}{V} = G_0 \left[1 + \frac{6m^* k_F}{\pi\hbar^2} \times \left(g + \frac{1}{2\mu_B} P_{\mathrm{eff}}(\varepsilon_F) J \cos\alpha \right) W(\mathbf{r}_0) \right]_{\varepsilon=\varepsilon_F}, \tag{58}$$

where G_0 is the conductance of the contact in absence of the cluster,

$$G_0 = (k_{F\uparrow}^2 + k_{F\downarrow}^2) \frac{e^2 \hbar^3 (k_F a)^4}{72\pi (m^* U_0)^2}, \tag{59}$$

$k_{F\sigma}$ is the magnitude of the Fermi wave vector in the magnetic metal for spin direction σ (see Eq. (56)), and

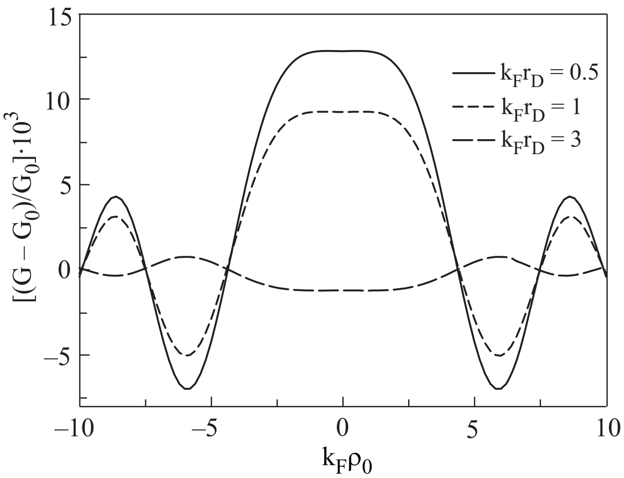

FIG. 7. The oscillatory part of the conductance as a function of tip position on a metal surface for subsurface magnetic clusters with different cluster diameters. The ρ-coordinate is measured from the point $\rho_0=0$ at which the contact is situated directly above the cluster; $r_0=(0,0,10)/K_F$; $g=0.5$; $J=(m^* k_F/\mu_B h^2) J\mu_{\rm eff}=2.5$; $P_{\rm eff}=0.4$; $\alpha=0$.[64]

$$W(\mathbf{r}_0)=\int d\mathbf{r}' D_0(|\mathbf{r}'-\mathbf{r}_0|)\left(\frac{z'}{r'}\right)^2 w(kr'). \tag{60}$$

The function w is defined by Eq. (29). When the radius of action r_D of the function $D_0(|\mathbf{r}-\mathbf{r}_0|)$ is much smaller than the distance between the contact and the center of the cluster, r_0, $W(\mathbf{r}_0)$ is an oscillatory function of kr_0 for $kr_D \geqslant 1$, as for a point defect with $kr_D \ll 1$ (see, Eq. (26) for $V=0$), but the oscillation amplitude is reduced as a result of superposition of waves scattered by different points of the cluster. The integral $W(\mathbf{r}_0)$ (60) can be calculated asymptotically for $r_0 \gg r_D$, $kr_0 \gg 1$, and $kr_D \gtrsim 1$. For a homogeneous spherical potential $D_0(|\mathbf{r}|)=V_D^{-1}\Theta(r_D-r)$ (V_D is the cluster volume), $W(\mathbf{r}_0)$ takes the form

$$W(\mathbf{r}_0)\simeq 3\left(\frac{z_0}{r_0}\right)^2 \frac{\sin 2kr_0}{(2kr_0)^2}\frac{j_1(kd)}{kd}, \tag{61}$$

where $d=2r_D$ is the cluster diameter. The last factor in Eq. (61) describes the quantum size effect connected with electron reflections at the cluster boundary. Oscillations of this sort can exist, if the cluster boundary is sharp (on the scale of the electron wave length). Figure 7 shows the dependence of the amplitude of the conductance oscillations on the cluster diameter. It demonstrates that a π-phase shift may take place as a result of interference of the electron waves over a distance on the order of the cluster diameter.

In Eq. (58) the term proportional to $P_{\rm eff}$ takes into account the difference in the probabilities of scattering of electrons with different σ by the localized magnetic moment $\mu_{\rm eff}$. It depends on the angle α between the tip magnetization and $\mu_{\rm eff}$, as $\cos\alpha$. The same dependence was first predicted for a tunnel junction between ferromagnets in which the magnetization vectors are misaligned by an angle α,[66] and this has been observed in SP-STM experiments.[24]

Note that once the spin-polarized current-induced torque pulls the magnetic moment away from alignment with H, the cluster moment will start precessing around the field axis. The Larmor frequency is determined by the magnetic field equal to the sum of the external field H and the effective

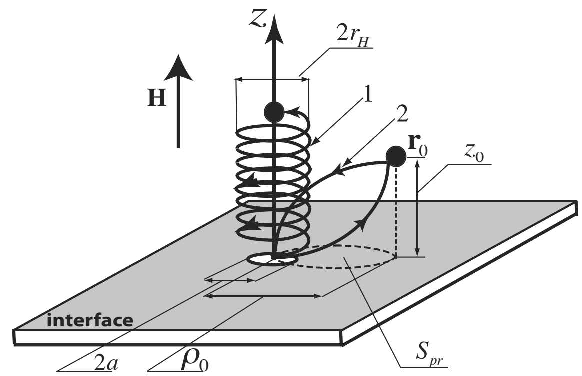

FIG. 8. Schematic representation of the electron trajectories in the vicinity of a point contact in an external magnetic field oriented along the contact axis.

magnetic field produced by the polarized current. The precession of the cluster magnetic moment gives rise to a time modulation of the SP-STM current, as in the case of clusters on a sample surface.[25,26]

VI. MAGNETO-QUANTUM OSCILLATIONS

A. Conductance oscillations in a perpendicular magnetic field

In a strong magnetic field the STM conductance exhibits characteristic oscillations in the magnetic field, which are attributed to Landau quantization. This effect has been observed in Ref. 67 and the energy dependence of the effective electron mass was found. The effect of a magnetic field on the interference pattern produced by two adatoms in STM conductance has been investigated theoretically[68] and horizontal stripes related to the Aharonov-Bohm effect were predicted.

In section III it was shown that $G(\mathbf{r}_0,V)$ undergoes oscillations in r_0 and eV owing to the variation of the phase shift between transmitted and scattered electron waves. Here we discuss another way of controlling the phase shift between the interfering waves: an applied external magnetic field $\mathbf{H}$ produces oscillations in the conductance that depend on H.

Let us consider the contact described in section II, now placed in a magnetic field directed along the contact axis, $\mathbf{H}=(0,0,H)$. Figure 8 illustrates the trajectories of the electrons that are injected into the metal and interact with the defect.

In the following, the Schrödinger equation is solved along the same lines as in section II, and as a zeroth approximation we use the well-known wave function for an electron in a homogeneous magnetic field. In Ref. 63 the dependence of the STM conductance on magnetic field has been obtained under the assumptions that the contact diameter a is much smaller than the magnetic quantum length, $a_H=\sqrt{\hbar/m^*\Omega}$, the radius of the electron trajectory, $r_H=\hbar k_F/m^*\Omega$, is much smaller than the mean free path of the electrons, $l \gg r_0$, and the separation between the magnetic quantum levels, the Landau levels, $\hbar\Omega$, is greater than k_BT ($\Omega=eH/m^*c$ is the Larmor frequency). Although these conditions severely restrict the possibilities for observing the oscillations, they can all be realized, e.g., in single crystals of semimetals (Bi, Sb and their ordered alloys) where the electron mean free path can be up to millimeters and the Fermi wave length $\lambda_F \sim 10^{-8}$ m. When the inequalities listed above are satisfied, the dependence of the conductance of the tunnel point contact on H is given by[63]

$$G(H)=G_c(H)\left[1+\frac{gm^*}{2\pi^3(N_{F\uparrow}+N_{F\downarrow})\hbar^2 a_H^4}\times\sum_\sigma\left(\mathrm{Im}\sum_{n=0}^{n_{\max}}\chi_\sigma(n,\mathbf{r}_0)\right)\left(\mathrm{Re}\sum_{n'=0}^{\infty}\chi_\sigma(n',\mathbf{r}_0)\right)\right]. \quad (62)$$

Here

$$\chi_\sigma(n,\mathbf{r}_0)=\exp\left(-\frac{\xi_0}{2}\right)L_n(\xi_0)\times\exp\left(\frac{i}{\hbar}z_0\sqrt{2m^*(\varepsilon_F+\sigma\mu_B H-\varepsilon_n)}\right), \quad (63)$$

$\xi_0=\rho_0^2/2a_H^2$, the $L_n(\xi)$ are Laguerre polynomials, $\varepsilon_n=\hbar\Omega(n+1/2)$, $\sigma=\pm 1$ is the spin index, $N_{F\sigma}$ is the number of electron states for one spin direction per unit volume at the Fermi energy, which is given by

$$N_{F\sigma}=\frac{2|e|H}{(2\pi\hbar)^2 c}\sum_{n=0}^{n_{\max}}\sqrt{2m^*(\varepsilon_F+\sigma\mu_B H-\varepsilon_n)}, \quad (64)$$

with $n_{\max}=[\varepsilon_F/\hbar\Omega]$ being the maximum quantum number n for which $\varepsilon_n<\varepsilon_F$, and $[x]$, the integral part of the number x, and G_c is the conductance in the absence of a defect,

$$G_c(H)=(\pi\hbar)^3\left(\frac{ea^2(N_{F\uparrow}+N_{F\downarrow})}{m^* U_0}\right)^2. \quad (65)$$

The conductance (65) undergoes oscillations with a periodicity corresponding to the de Haas-van Alphen effect, which originates from the step-wise dependence of the number of electron states $N_{F\sigma}$ (64) on the magnetic field. For $n_{\max}(\varepsilon_F)\gg 1$ and $\mu_B H/\varepsilon_F \ll 1$ (semiclassical approximation), Eq. (65) can be expanded in the small parameter $\hbar\Omega/\varepsilon_F$ as

$$G_c(H)\simeq G_0\left[1+\frac{9}{2}\left(\frac{\hbar\Omega}{\varepsilon_F}\right)^{3/2}\sum_{s=1}^{\infty}\frac{(-1)^s}{(2s)^{3/2}}\sin\left(2\pi s\frac{\varepsilon_F}{\hbar\Omega}-\frac{\pi}{4}\right)\right], \quad (66)$$

where G_0 is the conductance of the contact for $H=0$ (see Eq. (59)).

The oscillatory part of the conductance, $\Delta G(H)=G(H)-G_c(H)$, caused by electron scattering on the defect, is plotted in Fig. 9 for a defect located at $(\rho,z)=(50,30)/k_F$. Figure 10 illustrates the dependence of the conductance (62) on the coordinate ρ_0 of the defects for different H. The beating of the oscillation amplitude owing to the difference in electron energies for different spins is evident at higher magnetic fields.

The curve $G(H)$, (62), plotted in Fig. 9 contains oscillations with different periods. The semiclassical asymptotes of the expression (62) for the conductance at $\hbar\Omega\ll\varepsilon_F$ allow us to explain the physical origin of these oscillations. Using the

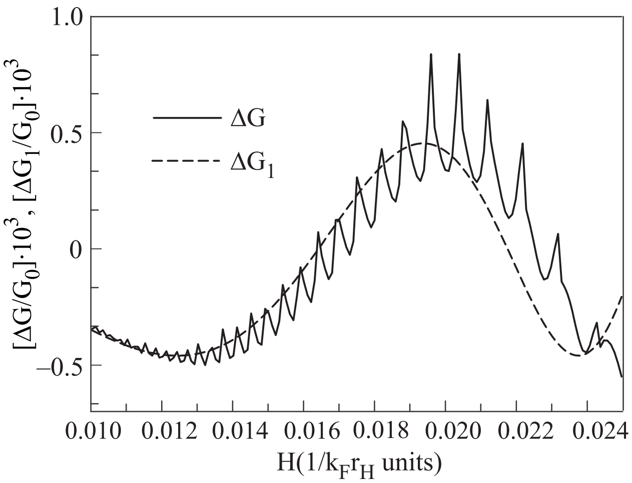

FIG. 9. Oscillatory part of the conductance of a tunneling point contact with a single defect placed at $k_F\rho_0=50$, $k_Fz_0=30$. The solid curve is a plot of Eq. (62), while the dashed curve shows the component ΔG_1 in the semiclassical approximation (68). The field scale is given in units of $1/k_F r_H$, and $\tilde{g}=0$.

Poisson summation formula in Eq. (62), the part of the conductance $\Delta G(H)$ related to scattering by the defect can be written as a sum of two terms

$$\Delta G(H)=\Delta G_1+\Delta G_2, \quad (67)$$

each of which describes conductance oscillations with different periods (to be discussed in more detail below).

B. Effect of quantization of the flux through the trajectories of scattered electrons

The first term $\Delta G_1(H,\mathbf{r}_0)$ in Eq. (67) describes the long-period oscillations

$$\Delta G_1(H,\mathbf{r}_0)=-G_0\tilde{g}\frac{z_0^2}{k_F^2 r_0^4}\sin\left(2k_F r_0-2\pi\frac{\Phi}{\Phi_0}\right), \quad (68)$$

where $\Phi_0-2\pi\hbar c/e$ is the quantum of flux. The flux, $\Phi-HS_{\mathrm{pr}}$, is produced by the field lines penetrating the projected areas S_{pr} on the plane $z=0$ of the trajectories of the electrons moving from the contact to the defect and back (see trajectory 2 in Fig. 8). These trajectories consist of two arcs, and there are many trajectories with different S_{pr}. As shown

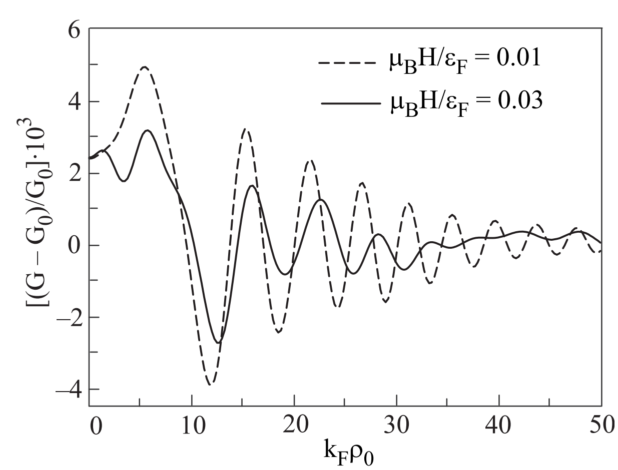

FIG. 10. The oscillatory part of the STM conductance as a function of tip position for different values of magnetic field; $z_0=30/k_F$, and $\tilde{g}=0.5$.

in Ref. 63, among these trajectories the signal is dominated by the one with a minimal area given by $S_{\mathrm{pr}}=2S_{\mathrm{seg}}$. Here $S_{\mathrm{seg}}=r^2(\theta-\sin 2\theta)$ is the area of the segment formed by the chord of length ρ_0 and the arc of radius $r=r_H \sin\theta$, with θ being the angle between the vector $\mathbf{r}_0$ and the z axis, i.e., $\sin\theta=\rho_0/r_0$. Therefore, the oscillation ΔG_1 vanishes when the defect lies on the contact axis, $\rho_0=0$. Obviously, these oscillations originate in the curvature of the electron trajectories in a magnetic field. As can be seen from Eq. (68), the oscillations in the conductance ΔG_1 are similar in nature to the Aharonov-Bohm effect (the conductance undergoes oscillations with a period Φ/Φ_0) and are related to the quantization of the magnetic flux through the area enclosed by an electron trajectory. As an illustration of this fact, in Fig. 9 the full expression for the oscillatory part $\Delta G(H)$ of the conductance (the second term in Eq. (62)) is compared with the semiclassical approximation $\Delta G_1(H,\rho_0,z_0)$ of Eq. (68).

For observation of Aharonov-Bohm-type oscillations the distance ρ_0 of the defect in the plane parallel to the interface must be shorter than r_H, i.e., the defect must be situated inside the "tube" of electron trajectories passing through the contact. At the same time, the inequality $\rho_0 > a_H$ must hold in order for a magnetic flux quantum Φ_0 be enclosed within the area of a closed trajectory.

C. Effect of longitudinal focusing of electrons onto a defect by a magnetic field

The short-period oscillations originate in focusing of the electrons by the magnetic field, and are described by the term $\Delta G_2(H,\mathbf{r}_0)$ in Eq. (67). For $\rho_0=0$ this term can be written as

$$\Delta G_2(H,z_0) \simeq \frac{1}{16} G_0 \tilde{g} \left(\frac{\hbar\Omega}{2\varepsilon_F}\right)^{3/2} \sum_{x=[z_0/2\pi r_H]}^{\infty} \frac{(-1)^s}{s^{3/2}} \times \cos\left(k_F r_0 + 2\pi s \frac{\varepsilon_F}{\hbar\Omega} + \frac{z_0^2}{4\pi s a_H^2}\right). \qquad (69)$$

In the absence of a magnetic field only those electrons that are scattered off the defect in a direction directly opposite to the incoming electrons can come back to the point contact. When $H \neq 0$ the electrons move along a spiral trajectory and may come back to the contact after scattering at a finite angle relative to the initial direction (trajectory 1 in Fig. 8). For example, if a defect is located on the contact axis, an electron moving from the contact with a wave vector $k_z=k_F$ along the magnetic field returns to the contact when the z-component of the momentum $k_{ss}=z_0 m^* \Omega/2\pi s h$, for integral s. For these orbits, the time of the motion over a distance z_0 in the z direction is a multiple of the cyclotron period $T_H=2\pi/\Omega$. Thus, after s orbits an electron returns to the contact axis at the point $z=0$. The phase which the electron acquires along its spiral trajectory is composed of two parts, i.e., $\Delta\phi=\Delta\phi_1+\Delta\phi_2$. The first, $\Delta\phi_1=k_{zs}z_0$, is the "geometric" phase accumulated by an electron with wave vector k_{zs} over the distance z_0. The second, $\Delta\phi_2=\pi s(eHr_s^2/ch)$, is the phase acquired during s orbits in the field H, where $r_s=\hbar c\sqrt{k_F^2-k_{zs}^2}/eH$ is the radius of the spiral trajectory. Substituting for k_{zs} and r_s in the equation for $\Delta\varphi$, we find

$$\Delta\phi = 2\pi s\varepsilon_F/\hbar\Omega + z_0^2/4\pi s a_H^2. \qquad (70)$$

This is just the phase shift that defines the period of the oscillations in the contribution ΔG_2 (69) to the conductance. It describes a trajectory which is straight for the part from the contact to the defect and spirals back to the contact in s orbits as shown in Fig. 8. There are trajectories consisting of helices along forward and reverse paths, with s and s' orbits, respectively. However, the contribution of these trajectories to the conductance is smaller than ΔG_2 (69) by a factor of $\sim 1/(k_F a_H) \ll 1$. Note that, although the amplitude of the oscillations in ΔG_2 (69) is smaller by a factor of $h\Omega/\varepsilon_F$ than the amplitude of the contribution from ΔG_1 (68), the first depends on the depth of the defect as $z_0^{-3/2}$, while $\Delta G_1 \sim z_0^{-2}$. The slower decrease in the amplitude for ΔG_2 is explained by focusing of the electrons in the magnetic field. The predicted oscillations, Eq. (69), are not periodic in H or in $1/H$. Their typical period can be estimated from the difference ΔH between two nearest-neighbor maxima,

$$\left(\frac{\Delta H}{H}\right) \simeq \frac{\hbar\Omega}{\varepsilon_F}\left[1-\left(\frac{z_0}{2\pi k_F a_H^2}\right)^2\right]^{-1}. \qquad (71)$$

The difference (period) (71) depends on the position of the defect. It is larger than the period of de Haas-van Alphen oscillation, $(\Delta H/H)_{\mathrm{dHvA}} \simeq \hbar\Omega/\varepsilon_F$. Both of these periods are of the same order of magnitude.

VII. NONMAGNETIC DEFECT IN A SUPERCONDUCTOR

In this section we present the results of a theoretical investigation of the conductance, G_{ns}, of a normal metal—superconductor (NS) point contact (with radius $a < \lambda_F$) in the tunneling limit and discuss the quantum interference effects originating from the scattering of quasiparticles by a point-like nonmagnetic defect.[69] The model is described in section II and illustrated in Fig. 1, modified by having the half-space $z>0$ occupied by a (s-wave) superconductor. At zero temperature, a tunnel current flows through the contact with an applied bias eV larger than the energy gap of the superconductor Δ_0. In order to evaluate the total current through the contact, $I(V)$, the current density $\mathbf{j}_\mathbf{k}(\mathbf{r})$ of quasiparticles with momentum $\mathbf{k}$ at $z>0$, formed by electrons transmitted through the contact, must be found. The current density $\mathbf{j}_\mathbf{k}(\mathbf{r})$ is expressed in terms of the coefficients $u_\mathbf{k}(\mathbf{r})$ and $v_\mathbf{k}(\mathbf{r})$ of the canonical Bogoliubov transformation.[70] The functions $u_\mathbf{k}(\mathbf{r})$ and $v_\mathbf{k}(\mathbf{r})$ satisfy the Bogoliubov-de Gennes (BdG) equations,[71] which must be supplemented with a self-consistency condition for the order parameter $\Delta(\mathbf{r})$, and with boundary conditions relating $u_\mathbf{k}$ and $v_\mathbf{k}$ in the normal metal to those in the superconductor at the contact. For a tunnel contact one can neglect Andreev reflections, because these lead to corrections to the conductance proportional to $|t|^4$;[72] the functions $u_\mathbf{k}$ and $v_\mathbf{k}$ satisfy the same boundary conditions (10) and (11) as the wave function for a contact between normal metals.

It is obvious that the method described in sections II and III can be generalized to NS contacts. As a first step the BdG equations must be solved in a linear approximation in the transmission amplitude t without a defect (D=0), after which the corrections owing to scattering by the defect can be found. In Ref. 69 an analytical solution for the BdG equations has been found in the approximation of a homogeneous order parameter $\Delta(\mathbf{r})-\Delta_0\Theta(z)$.

For small applied bias $eV \ll \hbar\omega_D \ll \varepsilon_F$ (ω_D is the Debye frequency) and in a linear approximation with respect to the electron—defect interaction constant g, the conductance G_{ns} of a NS tunnel point contact can be written as the sum of two terms,

$$G(V,r_0) = G_{0ns}(V) + \Delta G_{\text{osc}}(V,r_0), \quad eV > \Delta_0. \tag{72}$$

The first term, $G_{0ns}(V)$, in Eq. (72) is the conductance of the NS tunnel point contact with no defect

$$G_{0ns}(V) = G_0 N_s(eV), \tag{73}$$

where G_0 is the conductance of a contact between normal metals (27), which is multiplied by the normalized density of states of the superconductor $N_s(E)=E/\sqrt{D^2-\Delta_0^2}$ at $E=eV$. Although this sort of result is not unexpected and has been confirmed by experiment,[22] for a contact of radius $k_F a<1$ it was not obvious and was is first obtained in Ref. 69. The second term describes the oscillatory dependence of the conductance as a function of distance between the contact and the defect. If the defect is located in the superconductor ($z_0 <0$), then

$$\Delta G_{\text{osc}}(V,r_0) = - G_{0ns}(V)\tilde{g}\left(\frac{z_0}{r_0}\right)^2 \sum_{\alpha=\pm} \psi_\alpha(eV) w(k_\alpha r_0), \tag{74}$$

where

$$\psi_\pm(eV) = \frac{1}{2}\left(1 \pm \frac{\sqrt{(eV)^2-\Delta_0^2}}{eV}\right), \tag{75}$$

and

$$k_\pm = \frac{\sqrt{2m^*}}{h}[\varepsilon_F \pm \sqrt{(eV)^2-\Delta_0^2}]^{1/2}, \tag{76}$$

and the function $w(k_\alpha r_0)$ is given by Eq. (29). Equation (74) was derived by neglecting all small terms of order of Δ_0/ε_F and eV/ε_F. Note that we have retained the second term in square brackets in the equation for $k_\pm$ (76), because for large r_0 ($\sqrt{(eV)^2-\Delta_0^2}/\varepsilon_F)(k_F r_0) \simeq 1$, the phase shift of the oscillations may be important.

VIII. CONCLUSIONS

We have reviewed some theoretical aspects of the feasibility of investigating subsurface defects in STM experiments. The theory shows that the amplitude of the oscillations in the STM conductance resulting from quantum interference of electron waves injected by the STM tip and scattered by the defect is sufficiently large ($\sim 10^{-3}G_0$), even for defects located more than 10 atomic layers below the surface. For example, in the STM experiments of Ref. 73 signal-to-noise ratios of $5\cdot 10^4$ (at 1 nA, 400 Hz sample frequency) were achieved. Recently, the possibility of observing defects at these depths below a surface has been demonstrated experimentally in Ref. 33.

An STM tip serves as a "locator", which detects a defect below the metal surface by means of electron waves. The defect in turn yields information about its (defect) characteristics, and also reveals properties of the host metal by producing Friedel-like oscillations in the STM conductance. The phase of the oscillations, $2k_F r_0$, is defined by the Fermi wave vector k_F and the tip-defect distance r_0. One possibility for determining the depth z_0 of a defect below a surface is to change the maximum wave vector by accelerating the electrons with an applied bias eV.[47,74] When the tip is situated above a defect, the period of the oscillations in $G(V)$, $\Delta k_F(eV)z_0=\pi$, uniquely defines z_0. As the period of the oscillations becomes longer for smaller z_0 the minimum detectable depth will be determined by the maximum voltage that can be applied across the junction. For example, 30 mV is sufficient for probing a quarter of a conductance oscillation caused by a defect at 1 nm depth.

Another factor controlling the oscillation phase is the shape of the Fermi surface (FS). As shown above, for an anisotropic FS $\varepsilon(\mathbf{k})=\varepsilon_F$, the phase and amplitude of the conductance oscillations depend on the characteristics of the FS at the point for which the direction of the velocity $\mathbf{v}=\mathbf{v}_0$ is parallel to the vector $\mathbf{r}_0$ directed from the STM tip to the defect.[51] That is, the phase of the oscillations is determined by the projection of $\mathbf{k}$ on the direction of $\mathbf{v}_0$, and the oscillation amplitude depends on the curvature of the FS. Depending on the geometry of the FS, there can be several points with the same direction of the velocity, or, if the FS has open parts, certain directions of the velocity may be forbidden. It follows from the results above that plots of constant phase $\mathbf{k}\mathbf{v}_0 r_0/|\mathbf{v}_0|$ (maxima and minima) in the interference pattern of the STM conductance reveal the contours formed by projections of the vector $\mathbf{k}$ on the vector normal to the FS. Although such contours reflect the main features of the FS geometry, they cannot be regarded as a direct image of the FS.

Electron scattering by subsurface magnetic defects in STM conductance has some features distinct from scattering by magnetic adatoms and the shape and sign of the Kondo anomaly owing to a subsurface magnetic defect depend on depth.[46] Near a Kondo resonance the scattering phase shift δ_0 tends to $\pi/2$, and including multiple electron scattering events after reflections by the metal surface becomes essential. This explains the appearance of harmonics in the oscillatory part of the conductance, which have an additional phase shift $\Delta\phi=2(n-1)k_F z_0+n\delta_0$, where n is the number of electron reflections by the surface. The determination of this phase shift near the Kondo resonance ($V\simeq V_k$) and far from it (where $\delta_0\ll 1$) for the first ($n=0$) and second ($n=1$) harmonics provides an alternative way of determining the depth z_0 of a defect.

The possibilities of investigating magnetic defects are extended by injecting a spin-polarized current. If a subsurface cluster has an unscreened magnetic moment μ_{eff}, the scattering amplitudes for spin-up and spin-down electrons are different. This results in a dependence of the oscillation amplitude on the angle between the vector μ_{eff} and the polarization direction of the STM current; this is referred to as the magneto-orientational effect.[64]

A strong magnetic field perpendicular to the metal surface changes the interference pattern in the STM conductance fundamentally. Because of Zeeman splitting $\pm g_e\mu_B H$ of the Landau energy levels, the interference patterns in $G(\mathrm{r}_0)$ owing to electrons with different spin directions do not coincide since the electron wave lengths differ for the energies $\varepsilon_F \pm g_e \mu_B H$. The superposition of the two oscillatory parts may cause beating in the total amplitude of the oscillations. Along with the well-known quantum oscillations with a periodicity in H^{-1} from the de Haas-van Alphen effect in the STM conductance, when a defect is present two new types of oscillations are exist. The first is related to quantization of the flux through the projection of the electron trajectory onto the surface plane. The second type of oscillation, $G(H)$, is related to a focusing effect in the magnetic field. As in Sharvin's two-point contact experiments, where electrons were focused onto a collector by a magnetic field directed along the line connecting the contacts (longitudinal electron focusing),[75] a magnetic field can periodically focus the electrons injected by a tip onto a defect. This results in periodic variations in the part of the conductance related to scattering by a defect.[63]

When electrons tunnel from a normal-metal STM tip into a superconductor, the wave incident on the contact is transformed into a superposition of "electron-like" and "hole-like" quasiparticles. When a defect is located in the superconductor, quantum interference takes place between the transmitted partial wave and the partial wave that is scattered by the defect; this happens, independently, for both types of quasiparticles (Eq. (74)). Although the difference between the wave vectors $k^{(\pm)}(eV)$ of the "electrons" and "holes" is small, the shift $(k^{(+)}-k^{(-)})r_0$ between the two oscillations should be observable.[69]

[a]Email: kolesnichenko@ilt.kharkov.ua

[1] G. Binnig and H. Rohrer, IBM J. Res. Dev. **30**, 4 (1986).
[2] J. Friedel, Nuovo Cimento **7**, 287 (1958).
[3] J. M. Ziman, Principles of the Theory of Solids, Cambrige Univ. Press (1964).
[4] M. F. Crommie, C. P. Lutz, and D. M. Eigler, Nature (London) **363**, 524 (1993); Science **262**, 218 (1993).
[5] Y. Hasegawa and P. Avouris, Phys. Rev. Lett. **71**, 1071 (1993).
[6] L. Bürgi, N. Knor, H. Brune, M. A. Schneider, and K. Kern, Appl. Phys. **A75**, 141 (2002).
[7] L. Petersen, B. Schaefer, E. Lagsgaard, I. Stensgaard, and F. Besenbacher, Surf. Sci. **457**, 319 (2000).
[8] P. T. Sprunger, L. Petersen, E. W. Plummer, E. Lagsgaard, and F. Besenbacher, Science **275**, 1764 (1997).
[9] F. Vonau, D. Aubel, G. Gewinner, C. Pirri, J. C. Peruchetti, D. Bolmont, and L. Simon, Phys. Rev. B **69**, 081305(R) (2004).
[10] V. Madhavan, W. Chen, T. Jamneala, M. F. Crommi, and N. S. Wingreen, Science **280**, 567 (1998).
[11] J. Li, W.-D. Schneider, R. Berndt, and B. Delley, Phys. Rev. Lett. **80**, 2893 (1998).
[12] W. Chen, T. Jamneala, V. Madhavan, and M. F. Crommie, Phys. Rev. B **60**, R8529 (1999).
[13] N. Knorr, M. A. Schneider, L. Diekhöner, P. Wahl, and K. Kern, Phys. Rev. Lett. **88**, 096804 (2002).
[14] U. Fano, Phys. Rev. **124**, 1866 (1961).
[15] M. Plihal and J. W. Gadzuk, Phys. Rev. B **63**, 085404 (2001).
[16] P. Wahl, L. Diekhöner, M. A. Schneider, L. Vitali, G. Wittich, and K. Kern, Phys. Rev. Lett. **93**, 176603 (2004).
[17] H. P. Manoharan, C. P. Lutz, and D. M. Eigler, Nature (London) **403**, 512 (2000).
[18] G. A. Fiete and E. J. Heller, Rev. Mod. Phys. **75**, 933 (2003).
[19] O. Yu. Kolesnychenko, R. de Kort, M. I. Katsnelson, A. I. Lichtenstein, and H. van Kempen, Nature (London) **415**, 507 (2002).
[20] S. H. Pan, E. W. Hudson, K. M. Lang, H. Eisaki, S. Uchida, and J. C. Davis, Nature (London) **403**, 746 (2000).
[21] Ali Yazdani, B. A. Jones, C. P. Lutz, M. F. Crommie, and D. M. Eigler, Science **275**, 1767 (1997).
[22] S. H. Pan, E. W. Hudson, and J. C. Davis, Appl. Phys. Lett. **73**, 2992 (1998).
[23] M. Xu, Z. Xiao, M. Kitahara, and D. Fujita, Jpn. J. Appl. Phys., Part 2 **43**, 4687 (2004).
[24] M. Bode, Rep. Prog. Phys. **66**, 523 (2003).
[25] H. C. Manoharan, Nature (London) **416**, 24 (2002).
[26] C. Durkan and M. E. Welland, Appl. Phys. Lett. **80**, 458 (2002).
[27] O. O. Brovko and V. S. Stepanyuk, Phys. Status Solidi B 1-9 (2010).
[28] S. Crampin, J. Phys.: Condens. Matter **6**, L613 (1994).
[29] M. Schmid, W. Hebenstreit, P. Varga, and S. Crampin, Phys. Rev. Lett. **76**, 2298 (1996).
[30] O. Kurnosikov, O. A. O. Adam, H. J. M. Swagten, W. J. M. de Jonge, and B. Koopmans, Phys. Rev. B **77**, 125429 (2008).
[31] Yu Hongbin, C. S. Jiang, Ph. Ebert, and C. K. Shih, Appl. Phys. Lett. **81**, 2005 (2002).
[32] N. Quaas, M. Wenderoth, A. Weismann, R. G. Ulbrich, and K. Schönhammer, Phys. Rev. B **69**, 201103(R) (2004).
[33] A. Weismann, M. Wenderoth, S. Lounis, P. Zahn, N. Quaas, R. G. Ulbrich, P. H. Dederichs, and S. Blügel, Science **323**, 1190 (2009).
[34] W. A. Hofer, A. Foster, and A. Shluger, Rev. Mod. Phys. **75**, 1287 (2003).
[35] J. M. Blanco, F. Flores, and R. Pèrez, Prog. Surf. Sci. **81**, 403 (2006).
[36] I. O. Kulik, Yu. N. Mitsai, and A. N. Omelyanchouk, Zh. Eksp. Teor. Fiz. **63**, 1051 (1974).
[37] V. Bezàk, J. Math. Phys. **48**, 112108 (2007).
[38] V. Bezàk, Appl. Surf. Sci. **254**, 3630 (2008).
[39] A. V. Balatsky, I. Vekhter, and Jian-Xin Zhu, Rev. Mod. Phys. **78**, 373 (2006).
[40] V. S. Stepanyuk, A. N. Baranov, D. V. Tsivlin, W. Hergert, P. Bruno, N. Knorr, M. A. Schneider, and K. Kern, Phys. Rev. B **68**, 205410 (2003).
[41] E. L. Wolf, Principles of Electron Tunneling Spectroscopy, Oxford University Press, New York and Claredon Press, Oxford (1985).
[42] K. Kobayashi, Phys. Rev. B **54**, 17029 (1996).
[43] J. Tersoff and D. Hamann, Phys. Rev. B **31**, 805 (1985).
[44] I. M. Lifshits, M. Ya. Azbel', and M. I. Kaganov, Electron Theory of Metals, New York, Colsultants Bureau (1973).
[45] E. Granot and M. Ya. Azbel, Phys. Rev. B **50**, 8868 (1994); J. Phys.: Condens. Matter **11**, 4031 (1999).
[46] Ye. S. Avotina, Yu. A. Kolesnichenko, and J. M. Ruitenbeek, J. Phys.: Condens. Matter **20**, 115208 (2008).
[47] Ye. S. Avotina, Yu. A. Kolesnichenko, A. N. Omelyanchouk, A. F. Otte, and J. M. Ruitenbeek, Phys. Rev. B **71**, 115430 (2005).
[48] C. Untiedt, G. Rubio Bollinger, S. Vieira, and N. Agrat, Phys. Rev. B **62**, 9962 (2000).
[49] B. Ludoph, M. H. Devoret, D. Esteve, C. Urbina, and J. M. van Ruitenbeek, Phys. Rev. Lett. **82**, 1530 (1999).
[50] A. M. Kosevich, Fiz. Nizk. Temp. **11**, 1106 (1985) [Sov. J. Low Temp. Phys. **11**, 611 (1985)].
[51] Ye. S. Avotina, Yu. A. Kolesnichenko, A. F. Otte, and J. M. Ruitenbeek, Phys. Rev. B **74**, 085411 (2006).
[52] Yu. A. Aminov, Differential Geometry and Topology of Curves, Moskow, Nauka (1987) (in Russian).
[53] Ye. S. Avotina, Yu. A. Kolesnichenko, S. B. Roobol, and J. M. Ruitenbeek, Fiz. Nizk. Temp. **34**, 268 (2008) [Low Temp. Phys. **34**, 207 (2008)].
[54] Arthur P. Cracknell, *The Fermi Surfaces of Metals: a Description of the Fermi Surfaces of the Metallic Elements*, Taylor and Francis, London (1971).
[55] A. A. Abrikosov, *Fundamentals of the Theory of Metals*, North Holland (1988).
[56] M. A. Schneider, L. Vitali, N. Knorr, and K. Kern, Phys. Rev. B **65**, 121406 (2002).
[57] O. Újsághy, J. Kroha, L. Szunyogh, and A. Zawadowski, Phys. Rev. Lett. **85**, 2557 (2000).
[58] Chiung-Yuan Lin, A. H. Castro Neto, and B. A. Jones, Phys. Rev. B **71**, 035417 (2005).
[59] P. W. Anderson, Phys. Rev. **124**, 41 (1961).
[60] J. Frenkel and J. Dorfman, Nature (London) **126**, 274 (1930).
[61] S. V. Vonsovsky, Magnetism, John Wiley & Sons, New York (1974).
[62] F. J. Jedema, H. B. Heersche, A. T. Fllip, L. L. A. Baselmans, and B. J. van Weels, Nature (London) **416**, 713 (2002).
[63] Ye. S. Avotina, Yu. A. Kolesnichenko, A. F. Otte, and J. M. Ruitenbeek,

Phys. Rev. B **75**, 125411 (2007).
[64]Ye. S. Avotina, Yu. A. Kolesnichenko, and J. M. Ruitenbeek, Phys. Rev. B **80**, 115333 (2009).
[65]A. Kubetzka, M. Bode, O. Pietzsch, and R. Wiesendanger, Phys. Rev. Lett. **88**, 057201 (2002).
[66]J. C. Slonczewski, Phys. Rev. B **39**, 6995 (1989).
[67]M. Morgenstern, R. Dombrowski, Chr. Wittneven, and R. Wiesendanger, Phys. Status Solidi B **210**, 845 (1998).
[68]A. Cano and I. Paul, Phys. Rev. B **80**, 153401 (2009).
[69]Ye. S. Avotina, Yu. A. Kolesnichenko, and J. M. Ruitenbeek, Fiz. Nizk. Temp. **34**, 1184 (2008) [Low Temp. Phys. **34**, 936 (2008)].
[70]M. Hard, S. Datta, and P. F. Bagwell, Phys. Rev. B **54**, 6557 (1996).
[71]P. G. de Gennes, Superconductivity of Metals and Alloys W. A. Benjamin, Inc., New York (1966).
[72]G. E. Blonder, M. Tinkham, and T. M. Klapwijk, Phys. Rev. B **25**, 4515 (1982).
[73]B. C. Stipe, M. A. Rezaei, and W. Ho, Rev. Sci. Instrum. **70**, 137 (1999).
[74]Ye. S. Avotina, Yu. A. Kolesnichenko, and J. M. Ruitenbeek, J. Phys.: Conf. Series **150**, 022045 (2009).
[75]Yu. V. Sharvin, JETP Lett. **1**, 152 (1965).

This article was published in English in the original Russian journal. Reproduced here with stylistic changes by AIP.